

PHOTONS AND DILEPTONS AS PROBES OF EARLY-TIME
DYNAMICS IN RELATIVISTIC HEAVY-ION COLLISIONS

JESSICA CHURCHILL

Department of Physics
Faculty of Science
McGill University

April 2018

A thesis submitted to McGill University in partial fulfillment of the
requirements for the degree of Master of Science

©Jessica Churchill, April 2018

ABSTRACT

Vigorous experimental and theoretical programs are underway to study the behaviour of strongly interacting systems in extreme conditions of temperature and density. The only practical way to create such systems in terrestrial laboratories is to collide nuclei at relativistic energies. This is done at accelerator facilities such as the LHC (CERN, Geneva) and RHIC (Brookhaven National Laboratory, USA). These collisions of heavy ions contain so much energy in such a small volume that the colliding nuclei "melt" into a plasma of quarks and gluons. This creates an exotic form of nuclear matter: the quark-gluon plasma (QGP), which exists but for a fleeting moment, and can be studied through the particles that stream to the detectors. Two such particles are leptons and photons, which this research will focus on.

As it was discovered that the QGP can be very well modelled by relativistic fluid dynamics, there has been a large theoretical effort to completely characterize this QGP and understand its bulk properties. One of the aims of the McGill group is to obtain a value for the shear and bulk viscosities of the plasma: those are transport coefficients linked to fundamental properties of quantum chromodynamics (QCD), the theory of the nuclear strong interaction. The production of photons and dileptons can be used as probes to study these transport coefficients as they are emitted throughout the out-of-equilibrium evolution of the QGP medium, as well as within thermal equilibrium.

In order for such studies to be done, the electromagnetic signal from the pre-equilibrium phase needs to be quantified, which is the topic of this thesis. Using kinetic theory, the production rate of dileptons and photons was calculated for both thermal equilibrium and pre-equilibrium cases. In the thermal equilibrium case, results of the numerical integration of the differential dilepton and photon production rates were matched to the analytical solution. For the out-of-equilibrium case, transport equations derived within the diffusion approximation of the Boltzmann equation were solved numerically to study the thermalization of quarks and gluons in quark-gluon plasma.

RÉSUMÉ

Un vigoureux programme de recherche, à la fois expérimental et théorique, est actuellement en cours afin d'étudier le comportement, dans des conditions de température et pression extrêmes, les systèmes régis par l'interaction nucléaire forte. Le seul moyen pratique de créer de tels systèmes dans les laboratoires terrestres est la collision de noyaux atomiques à des niveaux d'énergie relativistes. Ceci est réalisé dans des accélérateurs tel que le LHC (CERN, Genève) et le RHIC (Brookhaven National Laboratory, USA). Ces collisions d'ions lourds possèdent une énergie telle que les noyaux « fondent » en un plasma de quarks et de gluons menant à la formation d'une forme exotique de la matière nucléaire : le plasma de quarks-gluons (Quark-Gluon Plasma, QGP). Ce dernier, n'existant que pour un instant fugace, peut être étudié par le truchement des particules mesurées par les détecteurs. Parmi ces particules, deux types sont les objets de ce projet de recherche : les leptons et les photons.

Alors qu'il a été découvert que le QGP peut être modélisé de manière convaincante en utilisant une version relativiste de la dynamique des fluides, un effort théorique important a été entrepris afin de le caractériser intégralement et de comprendre ses propriétés globales. L'un des objectifs du groupe à McGill est d'obtenir une valeur pour les viscosités de cisaillement et de volume. Ces dernières sont des coefficients de transports liées aux propriétés fondamentales de la chromodynamique quantique (Quantum Chromodynamics, QCD), la théorie liée à l'interaction nucléaire forte. La production de photons et de dileptons peut être utilisée afin de sonder les coefficients de transport alors que les particules sont émises de façon continue durant l'évolution du QGP.

Dans le but de réaliser ces études, le signal électromagnétique de la phase pré-équilibre doit tout d'abord être quantifié. Ceci est l'objet de cette thèse. Prenant appui sur une théorie cinématique, les taux de production de dileptons et de photons ont été calculés pour le cas à l'équilibre et hors d'équilibre. Dans le cas de l'équilibre thermal, les résultats de l'intégration numérique des taux de productions différentiels pour les dileptons et les

photons ont été comparés aux solutions analytiques. Pour la situation hors équilibre, les équations de transport dérivées dans le cadre de l'approximation dite « de diffusion » de l'équation de Boltzmann ont été résolues numériquement avec l'objectif d'étudier la thermalisation des quarks et des gluons dans le plasma.

ACKNOWLEDGEMENTS

Most importantly, I would like to thank my supervisor Charles Gale for his patience and dedication to my research. I would also like to thank Li Yan for his immeasurable contributions to establishing the groundwork for this thesis and for helping me overcome many of the computational issues which arose throughout this work. Thanks should also be given to Sangyong Jeon for his sage advice, to Alina Czajka for her helpful suggestions and friendship, and to all the members of my research group for their constructive feedback.

I would like also like to thank Matthew Heffernan for useful discussions, specifically during the painstaking phase space derivation and the many snack breaks we took as a result. Finally, I would like to thank my friends and family for continually supporting me.

CONTENTS

I	INTRODUCTION AND BACKGROUND INFORMATION	1
1	INTRODUCTION	3
1.1	Theory of Quantum Chromodynamics	3
1.2	Heavy-Ion Collisions	6
1.2.1	Simulations of Relativistic Heavy-Ion Collisions	8
1.3	Dilepton and Photon Production in Quark-Gluon Plasma	8
1.4	This Work	9
II	THE BOLTZMANN EQUATION	11
2	INTRODUCTION TO KINETIC THEORY	13
2.1	The Relativistic Boltzmann Equation	13
2.2	Rates in Kinetic Theory	15
2.3	Number and Energy Density	17
2.3.1	Number Density	17
2.3.2	Energy Density	18
3	SOLUTION TO THE BOLTZMANN EQUATION	19
3.1	Background Information	19
3.2	Transport Equations in a Quark-Gluon Medium	21
3.2.1	The Diffusion Approximation	21
3.2.2	Transport Equations for Spatially Homogeneous Systems	23
3.3	Thermodynamics of Quark-Gluon Plasma	25
3.4	Toward a Thermal QGP	26
III	CALCULATION OF THE PRODUCTION RATE AND YIELD OF DILEPTONS AND PHOTONS IN QGP	27
4	DILEPTON PRODUCTION IN THERMAL EQUILIBRIUM AND PRE-EQUILIBRIUM QGP	29

4.1	Dilepton Production Rate in Pre-Equilibrium QGP	29
4.2	Dilepton Production Rate in Thermal QGP	34
4.3	Comparison Between Thermal and Pre-Equilibrium Production Rates . . .	37
4.3.1	Ensuring consistency	37
4.3.2	Comparison	40
5	DILEPTON YIELD IN THERMAL EQUILIBRIUM AND PRE-EQUILIBRIUM QGP	45
5.1	Dilepton Yield in Pre-Equilibrium QGP	45
5.2	Dilepton Yield in Thermal QGP	46
5.3	Comparison Between Thermal and Pre-Equilibrium Yields	47
6	PHOTON PRODUCTION IN THERMAL EQUILIBRIUM AND PRE-EQUILIBRIUM QGP	49
6.1	Photon Production Rate in Pre-Equilibrium QGP	49
6.2	Photon Production Rate in Thermal QGP	52
6.3	Comparison Between Thermal and Pre-Equilibrium Production Rates . . .	59
7	PHOTON YIELD IN THERMAL EQUILIBRIUM AND PRE-EQUILIBRIUM QGP	63
7.1	Photon Yield in Pre-Equilibrium QGP	63
7.2	Photon Yield in Thermal QGP	64
7.3	Comparison Between Thermal and Pre-Equilibrium Yields	65
8	CONCLUSION	67
IV	APPENDIX	69
A	APPENDIX A	71
A.1	Energy Density - Maxwell-Boltzmann Statistics	71
A.2	Energy Density - Fermi-Dirac/Bose-Einstein Statistics	73
B	APPENDIX B	75
B.1	Number Density	75
	BIBLIOGRAPHY	77

LIST OF FIGURES

Figure 1	Phase diagram of quantum chromodynamics, taken from [3], which shows the phases of matter at extreme temperature T and density, represented by the chemical potential μ . The locations of quark-gluon plasma, color-flavor-locked (CFL) quark matter, neutron star matter, as well as ordinary matter such as hadrons are shown.	4
Figure 2	The strong coupling α_s as a function of the momentum transfer $Q = p_T$, taken from [5].	5
Figure 3	The various stages of heavy-ion collisions, taken from [12]. The evolution from the initial state of color-glass condensate (CGC) to the final process of hadronization and freeze-out into hadrons is shown. This thesis will focus on the pre-equilibrium glasma and thermalized quark-gluon plasma (QGP) stages.	7
Figure 4	Feynmanns diagram depicting the Born leading-order dilepton production through quark/anti-quark annihilation. Time runs from left to right.	9
Figure 5	Feynman diagram depicting the Born leading-order photon production via Compton scattering of a quark and gluon (left) and quark/anti-quark annihilation (right).	9
Figure 6	The temperature evolution plotted as a function of time for $Q_s = 1$ GeV.	39
Figure 7	The chemical potential evolution plotted as a function of time for $Q_s = 1$ GeV.	39

Figure 8	The pre-equilibrium dilepton production rate plotted for the timesteps $2/Q_s$, $12.5/Q_s$, and $25/Q_s$, which correspond to the temperatures 218 MeV, 160 MeV, and 140 MeV for $Q_s = 1$ GeV (left) and 436 MeV, 320 MeV, and 280 MeV for $Q_s = 2$ GeV (right). The dilepton invariant mass is set to $M = 3$ GeV in both cases.	41
Figure 9	The dilepton production rate in thermal equilibrium is plotted and compared to the pre-equilibrium rate calculated using the timestep $2/Q_s$ which corresponds to the same temperature. For $Q_s = 1$ GeV (left), the temperature $T = 218$ MeV and $T = 436$ MeV for $Q_s = 2$ GeV (right).	42
Figure 10	The number density of quarks and gluons in thermal equilibrium compared to that in the pre-equilibrium case computed using the methods described in Chapter 3 for $Q_s = 1$ GeV.	42
Figure 11	The ratio of the number density of thermal quarks/gluons to pre-equilibrium quarks/gluons (shown in blue) and the ratio of the number density of quarks to gluons in both the thermal and pre-equilibrium QGP (shown in orange) are compared for $Q_s = 1$ GeV.	43
Figure 12	The dilepton production rate in thermal equilibrium is plotted and compared to the pre-equilibrium rate as a function of time for both $Q_s = 1$ GeV (left) and $Q_s = 2$ GeV (right). In this plot, the values of both Q_\perp and M are taken to be 1 GeV.	43
Figure 13	The dilepton production rate as a function of mass in thermal equilibrium is plotted and compared to the pre-equilibrium rate calculated using the timestep $2/Q_s$. On the left $Q_s = 1$ GeV and on the right $Q_s = 2$ GeV.	44
Figure 14	The dilepton yield for the thermal and pre-equilibrium cases are plotted for $Q_s = 1$ GeV (left) and $Q_s = 2$ GeV (right).	47
Figure 15	The analytical solution of the thermal photon rate is plotted and compared to the numerical integration of equation 6.53 using $T = 200$ MeV.	57

Figure 16	The analytical solution of the thermal photon rate given by 6.65 is plotted and compared to the rate determined using the small-angle approximation given by 6.66 for $T = 200$ MeV. A value of $\mathcal{L} = 0.75$ was chosen to best match the two results.	58
Figure 17	The analytical solution of the thermal photon rate (eq. 6.65) is plotted and compared to the analytical solution (eq. 6.66) and the numerical integration of the rate (eq. 6.67) determined using small-angle approximation for a fixed $p_z = 0.5$ GeV.	58
Figure 18	The analytical solution of the thermal photon rate for a fixed $p_z = 0.5$ GeV (eq. 6.65) is plotted and compared to the analytical solution (eq. 6.66) and the numerical integration of the pre-equilibrium rate determined using small-angle approximation (eq. 6.21) for $Q_s = 1$ GeV, $T = 160$ MeV (left) and $Q_s = 2$ GeV, $T = 320$ MeV (right).	60
Figure 19	The photon production rate in thermal equilibrium is plotted and compared to the pre-equilibrium rate as a function of time for $Q_s = 1$ GeV (left) and $Q_s = 2$ GeV (right) with fixed $p_z, p_T = 0.5$ GeV.	61
Figure 20	The photon yield for the thermal and pre-equilibrium cases are plotted for $Q_s = 1$ GeV (left) and $Q_s = 2$ GeV (right) for a fixed value of $p_z = 0.5$ GeV.	65
Figure 21	The contribution to the thermal and pre-equilibrium photon yield from the Compton scattering and quark/anti-quark annihilation channels are compared to the total photon yield, the sum of these channels, for $Q_s = 1$ GeV and a fixed value of $p_z = 0.5$ GeV.	66
Figure 22	The temperature evolution as a function of τ for $Q_s = 1$ GeV (left) and $Q_s = 2$ GeV (right) is plotted in comparison with the temperature evolution given by the Bjorken solution.	72

Part I

INTRODUCTION AND BACKGROUND INFORMATION

The first section of this thesis serves as an introduction to important topics discussed and referenced throughout the work. Such topics include an introduction to quantum chromodynamics, heavy-ion collisions, and the formation of quark-gluon plasma. The motivation for this work as well as a brief overview are outlined.

INTRODUCTION

Approximately 13.7 billion years ago, just after the Big Bang, the universe was filled with an extremely hot and dense “soup” dominated by quarks and gluons, fundamental constituents of matter. This “soup”, referred to as quark-gluon plasma (QGP), existed only for a tiny fraction of a second, but is the origin from which all matter has been created. It is also theorized to possibly make up the interior of astrophysical bodies such as neutron stars and supernova as they are in similar states of extreme temperature and density, as shown in figure 1. Therefore, it is an important area of research for both nuclear physics and astronomy. However, it is impossible to recreate events such as the Big Bang and the astrophysical bodies are much too distant to analyze under controlled conditions. Thus, the only means of studying QGP on Earth is through its creation in the collision of large nuclei at relativistic energies, referred to as heavy ion collisions.

1.1 THEORY OF QUANTUM CHROMODYNAMICS

There are four known fundamental forces in existence: the gravitational and electromagnetic forces, as well as the strong and weak nuclear forces. However, the discovery of the W and Z bosons [1] elevated the weak interaction to the level of a gauge theory. This force is referred to as the electro-weak interaction and is a unified description of electromagnetism and the weak interaction.

When considering quark-gluon plasma, the most relevant of these forces is the strong nuclear force which governs the structure of hadrons such as protons and neutrons, the constituents of atomic nuclei. The strong force, mediated by gluons, is fundamentally

one of three possible colour "charges", namely the three primary colours of light, which are red, green, and blue. In contrast, anti-matter comes in either anti-red, anti-green, or anti-blue. At low temperatures and densities, the lower left corner of the diagram in figure 1, quantum chromodynamics dictates that quarks must form colourless hadrons [4]. As baryons have three valence quarks, this implies that they must contain three quarks of three different colours/anti-colours. Similarly for mesons which have two valence quarks, they must have one quark and one anti-quark of the same colour/anti-colour. Since gluons are also coloured particles, they interact among themselves as well with quarks. This causes the theory of QCD to become much more complicated than theories such as quantum electrodynamics (QED) as electromagnetic interactions are mediated by photons which, unlike gluons, do not carry charges themselves.

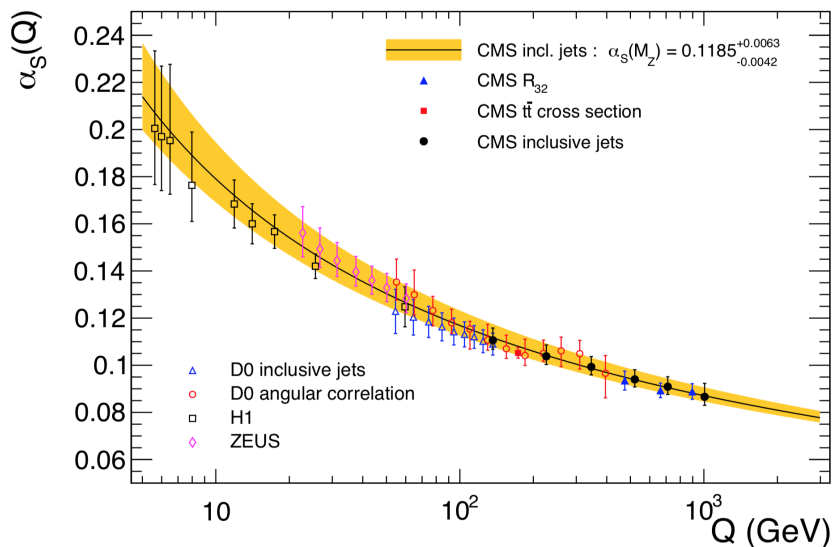


Figure 2: The strong coupling α_s as a function of the momentum transfer $Q = p_T$, taken from [5].

One of the main properties of QCD is how the strength of the force changes as a function of energy. The strength of the force is determined by what is known as a coupling constant, which in this case is the strong coupling constant $\alpha_s = g^2/4\pi$. Specifically, as shown in figure 2, α_s decreases asymptotically as the energy scale increases. This is referred to as "asymptotic freedom". As mentioned, quarks cannot be found in isolation at low temperatures and densities and must bind together to form colourless hadrons. This phenomena is termed "confinement". In this regime, the force is strong and therefore its properties are more difficult to calculate. At extreme temperatures and densities, the

strength of QCD is weaker, and quarks and gluons become asymptotically free under these conditions. This means that they can propagate over macroscopic distances and can then form quark-gluon plasma [2].

There are many approaches to studying QCD, two of which are perturbative QCD (pQCD) and lattice QCD. Perturbative QCD is used to study QCD at high energies as the strong coupling constant α_s is small in this region, thus allowing the application of perturbation techniques. This method, however, is invalid at low energies as α_s is large. Instead, this region is studied using lattice QCD where Feynman path integrals are evaluated numerically on a discrete space-time lattice [6]. This method can only give precise results for thermal QCD at zero net baryon density and is much more difficult to calculate in other regimes [7]. At temperatures around 200 MeV¹ [8], quarks and gluons are deconfined into quark-gluon plasma, but QCD is still strongly interacting. As this is the region of heavy ion collisions, it is therefore the focus of this thesis.

1.2 HEAVY-ION COLLISIONS

As mentioned, the only means of studying quark-gluon plasma here on Earth is through its creation in relativistic heavy-ion collisions. These experiments take place at both the Relativistic Heavy-Ion Collider (RHIC) at the Brookhaven National Laboratory and the Large Hadron Collider (LHC) at the European Organization for Nuclear Research, CERN. In these experiments, there is evidence to suggest that when heavy-ions such as gold (Au) and lead (Pb) are accelerated to relativistic speeds, they collide with one another with such high energy that the nuclei “melt” and form tiny droplets of QGP [9]. These QGP droplets exist for a fraction of a second before they cool and expand, causing them to form hadrons which fly off into detectors. The process, shown in figure 3, can be simplified into three main stages: pre-equilibrium and thermalization (which this thesis will focus on), hydrodynamics, and hadronization.

¹ In this thesis, natural units where $\hbar = c = k_B = 1$ were used throughout all calculations. Therefore, temperature is given in units of energy. Physical units were restored at the end of calculations. Additionally, the mostly negative Minkowski metric signature $(+, -, -, -)$ was used.

The pre-equilibrium stage refers to the medium created just after the two nuclei collide which initially consists almost entirely of gluons, sometimes referred to as "glasma" for gluon-plasma [10]. This medium evolves as quarks and anti-quarks are created until it eventually reaches a state of quark-gluon plasma close to thermal equilibrium. During this time, the quark-gluon plasma behaves as a fluid and can be modelled using hydrodynamics. The magnitude of the transport coefficients, shear and bulk viscosity, indicate that this is a nearly ideal fluid [11]. Shortly after this phase, as the system continues to cool, the temperature drops below the allowed temperature for quasi-free quarks and gluons to exist and they begin to bind together into hadrons. This process is known as hadronization, where the hadrons continue to interact until they "freeze-out". The following subsection describes in more detail how these stages are simulated.

It is important to note that pairs of quarks and anti-quarks are created throughout the evolution of these collisions which allow for both Compton scattering and quark/anti-quark annihilation to take place within the medium. Through these processes, photons and dileptons are produced which can be used as a probe to study the QGP. A description of how this is done is discussed in the next section.

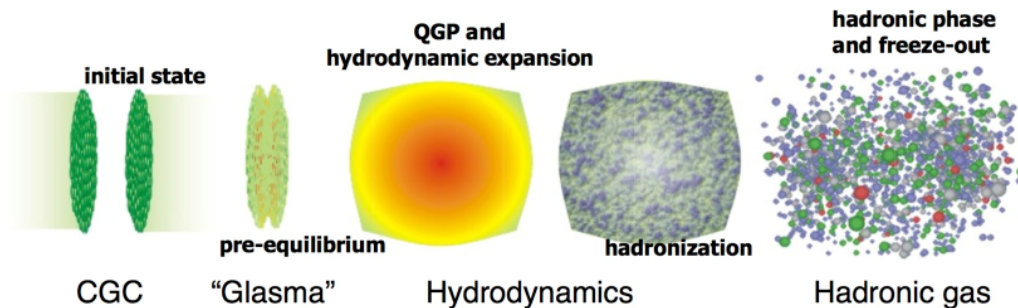


Figure 3: The various stages of heavy-ion collisions, taken from [12]. The evolution from the initial state of color-glass condensate (CGC) to the final process of hadronization and freeze-out into hadrons is shown. This thesis will focus on the pre-equilibrium glasma and thermalized quark-gluon plasma (QGP) stages.

1.2.1 *Simulations of Relativistic Heavy-Ion Collisions*

Relativistic hydrodynamics simulations of heavy-ion collisions are often used as a means of investigating and understanding QGP as it behaves like a near-ideal fluid. These simulations are first given a set of initial conditions, determined by the underlying physics of the nuclear wave function sampled at relativistic energies [13], which are then evolved using hydrodynamics. Studies continue to be successful in describing this medium using relativistic hydrodynamics, implying that the QGP formed in these collisions is close to thermal equilibrium. However, as the system is not quite an ideal fluid, assuming local thermal equilibrium and using ideal hydrodynamics is insufficient. Instead, a non-equilibrium viscous evolution of fluid dynamics is used with an equation of state taken from lattice QCD [14]. As the QGP cools and hadrons are formed, hydrodynamics is no longer valid due to the rapid expansion and growing mean-free paths, and the fluid must be converted into hadrons by sampling its momentum distribution [15]. These hadrons scatter [16] and fly off and are quantified by the simulation which can then be compared to experimental results.

1.3 DILEPTON AND PHOTON PRODUCTION IN QUARK-GLUON PLASMA

Since QGP is not a final state, but rather exists only for a brief period of time in the evolution of heavy-ion collisions, it cannot be studied directly. Therefore, a means of probing this medium is needed. Throughout the process of these collisions, both quarks and anti-quarks are created. Because of this, both Compton scattering and quark/anti-quark annihilation can take place. Shown in figures 4 and 5, these processes produce both dileptons and photons. This allows photons and dileptons to be used as probes to investigate the fluid. As they only interact with the medium electromagnetically, they are radiated throughout the entire course of the collision. In contrast, hadrons can also be used to study QGP. However, as they are produced as the medium cools and expands, they can only give complementary information about the later stages of QGP. Additionally, as hadrons are comprised of quarks and gluons, they interact very strongly with the medium. This means that they cannot escape the medium without undergoing sig-

nificant interactions with it. Owing to the relative size of the electromagnetic interaction, α_{EM}/α_s , photons and dileptons are able to easily escape the medium and can therefore give direct information about it, making them ideal probes for studying QGP.

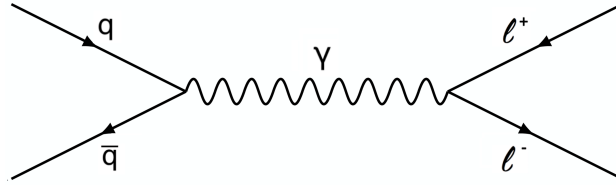


Figure 4: Feynmanns diagram depicting the Born leading-order dilepton production through quark/anti-quark annihilation. Time runs from left to right.

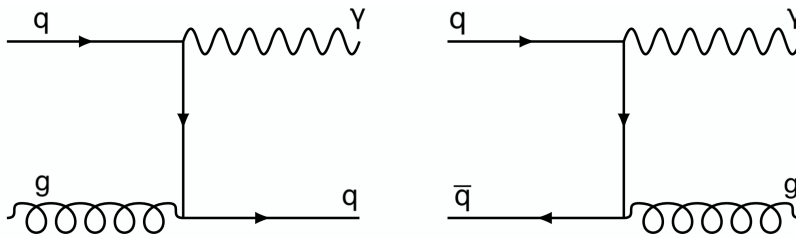


Figure 5: Feynman diagram depicting the Born leading-order photon production via Compton scattering of a quark and gluon (left) and quark/anti-quark annihilation (right).

Another reason photons and dileptons are useful probes of QGP is due to the fact that they are produced from many different sources such as through jets, radiation, and hadronic sources [17, 18]. However, this thesis will focus on those produced in both early times of heavy-ion collisions, as well as those produced once the medium has reached local thermal equilibrium.

1.4 THIS WORK

The purpose of this thesis is to use the production of dileptons and photons as a means of studying the very early quark-gluon plasma. Specifically, the production rates and yields of these particles are calculated using kinetic theory for early times of heavy-ion collisions. These calculations required the use of particle distribution functions determined computationally using an approach described in [19]. The results of these calculations

are then compared to that of the thermal case. The thermal production rates and yields are calculated using methods developed in [20] for photons and [21] for dileptons.

If the system of quarks and gluons is in thermal equilibrium, the particle distribution functions can be determined using either Maxwell–Boltzmann, Bose–Einstein, or Fermi–Dirac statistics. This thesis primarily uses Maxwell–Boltzmann statistics unless otherwise stated, meaning that all particle distribution functions are of the form $f(E) = e^{-E/T}$. However, deviations from the Maxwell-Boltzmann distributions were studied and will be discussed.

The following chapters of this thesis are organized as follows: Part II contains the necessary background information on kinetic theory, as well as the Boltzmann equation and how its solution yields the required particle distribution functions. Within this section, Chapter 2 gives an introduction to kinetic theory and how it is used to determine production rates of particles in addition to a derivation of the Boltzmann equation. Chapter 3 provides a discussion of the method of computing a solution to the Boltzmann equation and serves as a summary of the work presented in [19]. Part III is comprised of the results for the production rates and yields of the mentioned particles for both the thermal equilibrium and pre-equilibrium cases. Chapters 4 and 5 are dedicated to the dilepton calculations, whereas Chapters 6 and 7 contain the results for photons. Finally, the results of the thesis are summarized in Chapter 8 in Part IV.

Part II

THE BOLTZMANN EQUATION

This section provides an introduction to kinetic theory, as well as a detailed explanation of the Boltzmann equation and its derivation. Particle distribution functions and a computational method of solving the Boltzmann equation are also discussed.

INTRODUCTION TO KINETIC THEORY

Kinetic theory is the theory used to describe the physical properties of matter in terms of the particles within it. The fundamental equation in this theory is the Boltzmann equation, which describes the statistical behaviour of a thermodynamic system out of equilibrium. To understand its derivation, it is first important to define what is known as a distribution function. In the context of kinetic theory, a distribution function is a function that describes the number of particles per unit volume in a particular phase space location. The goal of kinetic theory is to determine these distribution functions knowing the form of the particle interactions and the initial conditions. These distribution functions are obtained as solutions to the Boltzmann equation.

In this thesis, particle distribution functions are primarily given in terms of either energy $f(E)$ or momentum $f(p_x, p_y, p_z, t) = f(p_\perp, p_z, t)$, where $p_\perp = (p_x, p_y)$ is the transverse momentum, p_z is the longitudinal momentum, and τ is the proper time. However, for the purposes of this derivation, the distribution function is given by $f(x, p)$, where x and p denote the position and momentum of the particle respectively.

2.1 THE RELATIVISTIC BOLTZMANN EQUATION

The two basic assumptions involved in the derivation of this equation are that collisions are events between only two particles which interact simultaneously and that they are distributed statistically. In heavy-ion collisions, the Boltzmann equation is often used to describe the underlying physics. Using the notation in [22] and [23], an overview of its derivation is presented as follows.

The focus of this derivation will be on the left-hand side of the Boltzmann equation as the right-hand side is only added to describe the effect of collisions between particles. The quantity $d^3\sigma_\mu$ is a time-like four vector which is a volume element of a plane space-

like surface σ , where $\Delta^3\sigma$ is a small segment at a point x . As mentioned, the distribution function used is given as $f(x, p)$ such that $f\Delta^3\sigma\Delta^3p$ describes the number of particles in the phase space segment $\Delta^3\sigma$ with momenta in the range Δ^3p about x, \mathbf{p} .

This derivation begins by first considering a gas in which each molecule is subject to an external force $F^\mu(x, p^\mu)$. In this notation, the superscript μ denotes a four-vector, such that $p^\mu = (p^0, p^1, p^2, p^3) = (E, p_x, p_y, p_z)$ and $F^\mu = \frac{\partial p^\mu}{\partial \tau} = (\frac{\partial E}{\partial \tau}, \frac{\partial \mathbf{p}}{\partial \tau})$. In the time $\Delta\tau$, it is assumed that all particles do not undergo a collision as the momentum of the particles changes from p^μ to $p^\mu + F^\mu\Delta\tau$ as it travels from the three-surface segment $\Delta^3\sigma$ to $\Delta^3\bar{\sigma}$. Given that there were no collisions after the time interval $\Delta\tau$, the exact same number of particles would be found in the three-surface segment $\Delta^3\bar{\sigma}$. Thus, the particle distribution function needs to be modified as

$$f(x, p) \rightarrow f(x, p^\mu + F^\mu\Delta\tau) \quad (2.1)$$

where the associated proper time interval is determined using the equation for the enclosed four-volume Δ^4x

$$\Delta^4x = \Delta\tau \frac{p^\mu}{m} \int_{\Delta^3\sigma} d^3\sigma_\mu. \quad (2.2)$$

If the number of particles crossing a segment $\Delta^3\sigma$ with momenta in the range Δ^3p around \mathbf{p} is given by

$$\Delta N(x, p) = \int_{\Delta^3\sigma} \int_{\Delta^3p} d^3\sigma_\mu d^3p f(x, p), \quad (2.3)$$

the number of particles crossing the segment $\Delta^3\bar{\sigma}$ sometime later is

$$\int_{\Delta^3\bar{\sigma}} \int_{\Delta^3p} d^3\sigma_\mu \frac{d^3p}{p^0} p^\mu f(x, p) - \int_{\Delta^3\sigma} \int_{\Delta^3p} d^3\sigma_\mu \frac{d^3p}{p^0} p^\mu f(x, p) = 0. \quad (2.4)$$

In the case of the external force, this becomes

$$\int_{\Delta^3\bar{\sigma}} \int_{\Delta^3p} d^3\sigma_\mu \frac{d^3p}{p^0} p^\mu f(x, p^\mu + F^\mu\Delta\tau) - \int_{\Delta^3\sigma} \int_{\Delta^3p} d^3\sigma_\mu \frac{d^3p}{p^0} p^\mu f(x, p) = 0. \quad (2.5)$$

After a Taylor expansion and the application of Gauss' theorem,

$$\Delta^4x \frac{\Delta^3p}{p^0} \left[p^\mu \partial_\mu + mF^\mu(x, p) \frac{\partial}{\partial p^\mu} \right] f(x, p) = 0, \quad (2.6)$$

where $\partial_\mu = \partial/\partial x^\mu$. Assuming the function is smooth, this can be written as

$$\int_{\Delta^4x} \int_{\Delta^3p} d^4x \frac{d^3p}{p^0} \left[p^\mu \partial_\mu + mF^\mu(x, p) \frac{\partial}{\partial p^\mu} \right] f(x, p) = 0, \quad (2.7)$$

Thus, the equation

$$p^\mu \partial_\mu + mF^\mu(x, p) \frac{\partial}{\partial p^\mu} f(x, p) = 0 \quad (2.8)$$

is deduced for the collisionless case. In the presence of collisions, this is modified as

$$p^\mu \partial_\mu + mF^\mu(x, p) \frac{\partial}{\partial p^\mu} f(x, p) = C(x, p) \quad (2.9)$$

where $C(x, p)$ is the collision term which accounts for particles which may have entered or left the volume element after having undergone a collision. This term, sometimes written as R_{coll} , describes the rate of collisions between particles and is discussed further in the next section.

2.2 RATES IN KINETIC THEORY

Throughout the derivation of the left-hand side of the Boltzmann equation presented in the previous section, it was assumed that there were no collisions occurring between particles. Conversely, the term on the right-hand side of the equation is introduced purely to account for particles that have undergone collisions which may enter or leave the volume element of the phase space. This term is referred to as the collision term and is denoted as either $R_{coll}(\mathbf{x}, \mathbf{p})$ or $\mathcal{C}[f_{\mathbf{p}}^i]$ depending on the notation. It is such that $R_{coll} d^4x d^3p / p^0$ is the average change of the number of particles having momenta between \mathbf{p} and $\mathbf{p} + d\mathbf{p}$ in the four-volume d^4x at a given space-time point x .

The number of collisions per unit volume and per unit time at the space-time point x is obtained using the assumption that the particles interact only within a short range. In this assumption, the interactions of these particles can be described by $f(\mathbf{x}, \mathbf{p})$ which does not vary significantly over the interaction distance. If the collision occurs such that $(\mathbf{p}, \mathbf{p} + d\mathbf{p}), (\mathbf{p}_1, \mathbf{p}_1 + d\mathbf{p}_1) \rightarrow (\mathbf{p}', \mathbf{p}' + d\mathbf{p}'), (\mathbf{p}'_1, \mathbf{p}'_1 + d\mathbf{p}'_1)$, the total loss of particles having momenta $(\mathbf{p}, \mathbf{p} + d\mathbf{p})$ in the space-time volume d^4x is obtained by multiplying

by d^4x and integrating over the final momenta \mathbf{p}' , \mathbf{p}_1 and the momentum of the collision partner \mathbf{p}_1 . Thus, the expression for $R_{coll}(\mathbf{x}, \mathbf{p})$ can be written as

$$R_{coll} = \mathcal{N} \int \frac{d^3p}{2p^0(2\pi)^3} \frac{d^3p_1}{2p_1^0(2\pi)^3} f_p(\mathbf{x}, \mathbf{p}) f_{p_1}(\mathbf{x}, \mathbf{p}_1) (2\pi)^4 \delta(p^\mu + p_1^\mu - p'^\mu - p_1'^\mu) \\ \times |\mathcal{M}_i|^2 \frac{d^3p'}{2p'^0(2\pi)^3} \frac{d^3p_1'}{2p_1'^0(2\pi)^3} [1 \pm f_{p'}(\mathbf{x}, \mathbf{p}')] [1 \pm f_{p_1'}(\mathbf{x}, \mathbf{p}_1')], \quad (2.10)$$

where $|\mathcal{M}_i|^2$ is the amplitude for a particular interaction i , \mathcal{N} is a degeneracy factor, and the \pm in the distribution function of the particle in the final state accounts for either a Bose-enhancement or a Pauli-suppression. For dilepton production from particle/anti-particle annihilation, for example, the rate of production can be written as [21]

$$R(a^+a^- \rightarrow l^+l^-) = \int \frac{d^3p_1}{(2\pi)^3 E_1} f(\mathbf{p}_1) \int \frac{d^3p_2}{(2\pi)^3 E_2} f(\mathbf{p}_2) v_{rel} \sigma(a^+a^- \rightarrow l^+l^-; \mathbf{p}_1 \mathbf{p}_2) \quad (2.11)$$

where $f(\mathbf{p}_1)$ and $f(\mathbf{p}_2)$ are the distribution function of particles 1 and 2, the degeneracy factor \mathcal{N} is absorbed into the interaction cross-section σ , and the relative velocity between the particles is given by

$$v_{rel} = \frac{\sqrt{p_1 \cdot p_2 - m_a^4}}{E_1 E_2}. \quad (2.12)$$

In the case of a photon producing reaction, the rate of production is given by [2]

$$R(1+2 \rightarrow 3+\gamma) = \mathcal{N} \int \frac{d^3p_1}{(2\pi)^3 2E_1} \frac{d^3p_2}{(2\pi)^3 2E_2} f_1(E_1) f_2(E_2) (2\pi)^4 \delta^4(p_1 + p_2 - p_3 - p_\gamma) \\ \times |\mathcal{M}_i|^2 \frac{d^3p_3}{(2\pi)^3 2E_3} \frac{d^3p_\gamma}{2E(2\pi)^3} [1 \pm f_3(E_3)]. \quad (2.13)$$

In the above equations, R denotes the number of collisions per unit space-time. Thus, it can be expanded as $R = dN/d^4X$, where d^4X is the space-time volume element. This volume element can be further expanded as $d^4X = \tau d\tau d\eta d^2x_\perp$ [24]. In this expansion, d^2x_\perp is the transverse area of the collision with the coordinate $x_\perp = (x, y)$ and the space-time rapidity $\eta = \text{arctanh}(z/t)$ describes the angle between the particle in position space and the positive direction of the beam axis where z is the angular dependence. In a longitudinally expanding system [24], the proper time τ is given as $\tau = \sqrt{t^2 - z^2}$.

In a later chapter of this thesis, it is shown how the above rates can be converted from total rates to differential ones by inserting a δ^4 -function and rewriting as dR/d^4Q in the case of the dilepton production rate, or rearranging the photon production rate

such that it can be written as EdR/d^3p . Again, the expression for these rates can be written using $R = dN/d^4X$. However, these expressions can be further expanded as $d^4Q = MdMdyd^2Q_\perp$ and $d^3p/E = dyd^2p_\perp$. In this notation, the center-of-mass energy is denoted by M , the transverse momentum $Q_\perp = (Q_x, Q_y)$, and the momentum rapidity is given by $y = \text{arctanh}(p_z/E)$ which is related to the angle between the particle three-momentum \mathbf{p} and the positive direction of the beam axis. These expansions are used later for converting from production rates to yields of dileptons and photons.

2.3 NUMBER AND ENERGY DENSITY

In this section, the kinetic theory definition of two useful concepts known as number density and energy density are discussed. These concepts are used to quantify the number of particles and the amount of energy contained in a system. In the following subsections, the equations for calculating these quantities are derived.

2.3.1 Number Density

Number density is defined as the number of particles per unit volume at a specific space-time location. The expression for the number density can be derived from the particle four-flow given by the equation

$$N^\mu = \sum_{k=1}^N c_k \int \frac{d^3\mathbf{p}_k}{(2\pi)^3 p_k^0} p_k^\mu f_k(\mathbf{p}_k, \tau). \quad (2.14)$$

The number density is defined as the 0^{th} component of N^μ

$$N^0 = \sum_{k=1}^N c_k \int \frac{d^3\mathbf{p}_k}{(2\pi)^3} f_k(\mathbf{p}_k, \tau) \quad (2.15)$$

which is simply the integral over the distribution function in the volume element [22]. In this equation, the coefficient c_k is used to denote potential degeneracy factors. Thus, in the case of a two-species ensemble, this expression becomes

$$n(\tau) = c_1 \int \frac{d^3\mathbf{p}_1}{(2\pi)^3} f_1(\mathbf{p}_1, \tau) + c_2 \int \frac{d^3\mathbf{p}_2}{(2\pi)^3} f_2(\mathbf{p}_2, \tau), \quad (2.16)$$

which can be written as

$$n(\tau) = \nu_g \int \frac{d^3 \mathbf{p}}{(2\pi)^3} f_g(\mathbf{p}, \tau) + \nu_q \int \frac{d^3 \mathbf{p}}{(2\pi)^3} f_q(\mathbf{p}, \tau) \quad (2.17)$$

if the particles considered are quarks and gluons. Anti-quarks are treated in the same manner as quarks, so they have been absorbed into ν_q as an additional factor of 2.

2.3.2 Energy Density

Energy density describes the amount of energy contained in a given system or region of space per unit volume. The expression for energy can be derived starting with the energy-momentum tensor

$$T^{\mu\nu}(\tau) = \sum_{k=1}^N c_k \int \frac{d^3 \mathbf{p}_k}{(2\pi)^3 p_k^0} p_k^\mu p_k^\nu f_k(\mathbf{p}_k, \tau) \quad (2.18)$$

which is used to describe the density and flux of energy and momentum in spacetime. The energy density is determined when $\mu, \nu = 0$. Again, in the case of a two-species ensemble,

$$T^{00}(\tau) = c_1 \int \frac{d^3 \mathbf{p}_1}{(2\pi)^3} p_1^0 f_1(\mathbf{p}_1, \tau) + c_2 \int \frac{d^3 \mathbf{p}_2}{(2\pi)^3} p_2^0 f_2(\mathbf{p}_2, \tau), \quad (2.19)$$

which, for quarks and gluons, becomes

$$\epsilon(\tau) = \nu_g \int \frac{d^3 \mathbf{p}}{(2\pi)^3} p^0 f_g(p^0, \tau) + \nu_q \int \frac{d^3 \mathbf{p}}{(2\pi)^3} p^0 f_q(p^0, \tau). \quad (2.20)$$

SOLUTION TO THE BOLTZMANN EQUATION

In order to compute production rates of particles from the equations in the previous section, the particle distribution functions must first be determined. This becomes complicated when the particles are not in thermal equilibrium. In this case, they must be determined by solving the Boltzmann equation. As this thesis focuses on the comparison between particle production rates and yields in thermal equilibrium versus pre-equilibrium, the out-of-equilibrium distribution functions are essential. This becomes additionally complicated in the case of heavy ion collisions as the system is rapidly evolving, and therefore the distribution of particles changes as a function of time. However, a method of numerically calculating these distribution functions was determined by [19]. This chapter is dedicated to describing the procedure required for this calculation.

3.1 BACKGROUND INFORMATION

In the very early stages of a relativistic heavy ion collision, a dense system consisting almost entirely of gluons is theorized to exist [25]. The comparatively large population of gluons is also conserved in the phenomenologically-extracted parton distribution functions [26]. This system is produced in a time scale of order $t \sim 1/Q_s$, where Q_s is the saturation momentum which characterizes the initial wave functions of the nuclei [27]. The gluons present in this initial state having momentum $p \lesssim Q_s$ have an occupation number f_0 which could be as large as $1/\alpha_s$, where α_s is the strong coupling constant which determines the strength of the strong interaction.

As the system thermalizes, there has been evidence to suggest that a Bose-Einstein condensate (BEC) could develop [28, 29]. However, whether or not a transient BEC emerges is beyond the scope of this work. Instead, the effects of inelastic processes which cause a variation in the number of gluons are studied as they can lead to the creation of

quark/anti-quark pairs. In this work, $q\bar{q}$ pairs are formed by gluon fusion. The inverse reaction is also included.

Initially after heavy ion collisions, the medium created contains a negligible amount of quarks and anti-quarks in comparison with the large number of gluons present. This will become evident in figure 10 where it is clearly shown that the number density of gluons vastly outweighs that of quarks/anti-quarks at very early times. In contrast, quarks and anti-quarks account for about 66% of the energy density of thermalized quark-gluon plasma, where the equation is given by

$$\epsilon = 3P = \left[16 + \frac{21}{2}N_f\right] \frac{\pi^2}{30} T^4, \quad (3.1)$$

so the evolution of this medium as it thermalizes from a dense system of gluons is important to study. In this equation, N_f (taken as $N_F = 3$ by RHIC and LHC) is the number of flavours of massless quarks/anti-quarks, T is the temperature, and it is assumed that quarks and gluons are non-interacting. If $N_f = 3$, the equation reduces to equation A.19.

The total number of gluons in the system is decreased through the production of quarks. As the total number of partons are conserved in the processes included in the Boltzmann equation, a chemical potential develops as the system evolves. Assuming that the initial number of gluons is not too large, this situation is denoted as under-population. In contrast, if the initial number of gluons is large enough, the situation of over-population occurs.

In order to study the evolution towards thermal equilibrium, two coupled kinetic equations, transport equations, for both gluons and quarks/anti-quarks are needed. These are obtained using the Boltzmann equation in the diffusion approximation with the assumption that all scatterings are small angle scatterings [30]. The collision term used contains only $2 \leftrightarrow 2$ processes between quarks and gluons and all other processes are neglected. The baryon number density is set to zero, therefore, quarks and anti-quarks are described using the same transport equation. This transport equation is coupled to that of gluons and solved numerically. The details of this solution are described in the following sections.

3.2 TRANSPORT EQUATIONS IN A QUARK-GLUON MEDIUM

To study the evolution of the medium created in relativistic heavy ion collisions, a description of quark and gluon degrees of freedom in terms of phase space distributions is required. These colour and spin averaged distribution functions are denoted as $f(t, \mathbf{x}, \mathbf{p})$ for gluons and $F(t, \mathbf{x}, \mathbf{p})$ for quarks. As anti-quarks are treated in the same manner as quarks, their distribution functions are the same. In a thermal bath of quarks and gluons, the amount of quarks and gluons having thermal masses larger than the temperature T is negligible compared to the amount of light quarks and gluons. Therefore, only light quarks and gluons are considered and they are taken to be massless for simplicity. Additionally, it is assumed that the baryon number density is small (taken to be zero) and there are no external forces exerted on the partons.

3.2.1 The Diffusion Approximation

The Boltzmann equation is used to describe the evolution of the phase space distribution function. It can be written as

$$D_t f_{\mathbf{p}}^a \equiv \left(\frac{\partial}{\partial t} + \mathbf{v} \cdot \nabla_x \right) f_{\mathbf{p}}^a = \mathcal{C}[f_{\mathbf{p}}^a] \quad (3.2)$$

where D_t is the covariant derivative, $\mathcal{C}[f_{\mathbf{p}}^a]$ is the collision term, and $f_{\mathbf{p}}^a$ is the distribution function of different species denoted by the superscript a . This collision term includes all $2 \leftrightarrow 2$ scattering processes from QCD and takes the form

$$\begin{aligned} \mathcal{C}[f_{\mathbf{p}}^a] = & \frac{1}{2E_p v_a} \sum_{b,c,d} \frac{1}{s_{cd}} \int \frac{d^3 \mathbf{p}'}{(2\pi)^3 2E_{\mathbf{p}'}} \frac{d^3 \mathbf{k}}{(2\pi)^3 2E_{\mathbf{k}}} \frac{d^3 \mathbf{k}'}{(2\pi)^3 2E_{\mathbf{k}'}} (2\pi)^4 \delta^4(P + P' - K - K') \\ & \times |\mathcal{M}_{cd}^{ab}|^2 [f_{\mathbf{k}}^c f_{\mathbf{k}'}^d (1 + \epsilon_a f_{\mathbf{p}}^a) (1 + \epsilon_b f_{\mathbf{p}'}^b) - f_{\mathbf{p}}^a f_{\mathbf{p}'}^b (1 + \epsilon_c f_{\mathbf{k}}^c) (1 + \epsilon_d f_{\mathbf{k}'}^d)], \quad (3.3) \end{aligned}$$

where the degeneracy factor v_a represents the spin and colour degrees of freedom and corresponds to the average over the initial state of particle a given as $v_a = 2(N_c^2 - 1)$ for gluons and $v_a = 2N_c$ for quarks/anti-quarks. Additionally, ϵ_a is used to distinguish between fermions and bosons, taking $\epsilon_a = 1$ for bosons and $\epsilon_a = -1$ for fermions, and s_{cd} is a symmetry factor. Furthermore, a and b denote incoming particles, and outgoing particles are denoted by c and d .

In a medium consisting almost entirely of gluons, the differential cross-section $gg \leftrightarrow gg$ diverges if the transferred momentum \mathbf{q} is significantly smaller than that of the two scattering gluons. Thus, the system is dominated by low momentum transfer or small angle scatterings. This allows for the Boltzmann equation to be treated in a diffusion approximation, so a Fokker-Planck equation [31] can then be used

$$D_t f = -\nabla_{\mathbf{p}} \cdot \mathcal{J} \quad (3.4)$$

where \mathcal{J} is an effective current due to the small angle collisions which is proportional to the integral

$$\mathcal{L} \simeq \int_{q_{min}}^{q_{max}} \frac{dq}{q}. \quad (3.5)$$

In this equation, the lower bound q_{min} is of the order of the screening mass [32] and the upper bound q_{max} is of the order of the largest momentum in the system.

Conversely, in a system consisting of both quarks and gluons, the small angle scatterings of both $q\bar{q}$ and $qg/\bar{q}g$ must also be considered. Therefore, there are two additional currents denoted as \mathcal{J}_g for gluons and \mathcal{J}_q for quarks. The processes $q\bar{q} \leftrightarrow gg$, $qg \leftrightarrow qg$, and $\bar{q}g \leftrightarrow \bar{q}g$ contribute to the source terms \mathcal{S}_g for the production of gluons, and \mathcal{S}_q for the production of quarks. From this, two diffusion-like equations are obtained

$$D_t f = -\nabla_{\mathbf{p}} \cdot \mathcal{J}_g + \mathcal{S}_g \quad (3.6)$$

$$D_t F = -\nabla_{\mathbf{p}} \cdot \mathcal{J}_q + \mathcal{S}_q \quad (3.7)$$

which have the currents

$$\mathcal{J}_g = -4\pi\alpha_s^2 N_c \mathcal{L} \left[\mathcal{I}_a \nabla_{\mathbf{p}} f + \mathcal{I}_b \frac{\mathbf{p}}{p} f(1+f) \right] \quad (3.8)$$

$$\mathcal{J}_q = -4\pi\alpha_s^2 C_F \mathcal{L} \left[\mathcal{I}_a \nabla_{\mathbf{p}} F + \mathcal{I}_b \frac{\mathbf{p}}{p} F(1-F) \right] \quad (3.9)$$

and the sources are

$$\mathcal{S}_g = \frac{4\pi\alpha_s^2 C_F N_f \mathcal{L} \mathcal{I}_c}{p} [F(1+f) - f(1-F)] \quad (3.10)$$

$$\mathcal{S}_q = -\frac{4\pi\alpha_s^2 C_F^2 \mathcal{L} \mathcal{I}_c}{p} [F(1+f) - f(1-F)] \quad (3.11)$$

with

$$\mathcal{I}_a = \int \frac{d^3\mathbf{p}}{(2\pi)^3} [N_c f(1+f) + N_f F(1+F)] \quad (3.12)$$

$$\mathcal{I}_b = 2 \int \frac{d^3\mathbf{p}}{(2\pi)^3} \frac{1}{p} (N_c f + N_f F) \quad (3.13)$$

$$\mathcal{I}_c = \int \frac{d^3\mathbf{p}}{(2\pi)^3} \frac{1}{p} (f + F). \quad (3.14)$$

In the above equations, C_F is the square of the Casimir operator of the colour $SU(N_c)$ group in the fundamental representation and is given by $C_F = (N_c^2 - 1)/(2N_c)$. For the derivations of these equations, see Appendix A of [19].

3.2.2 Transport Equations for Spatially Homogeneous Systems

In a spatially homogeneous system of quarks and gluons, the spatial dependence of the phase space distribution can be ignored, thus $D_t = \frac{\partial}{\partial t}$, and the momentum distributions are assumed to be isotropic. A new time variable is then introduced

$$\tau = \frac{2\alpha_s^2 N_c \mathcal{L}}{\pi} t. \quad (3.15)$$

With this, equations 3.6 and 3.7 can be rewritten as

$$\dot{f} = -\frac{1}{p^2} (p^2 J_g)' + \frac{C_F N_f}{N_c} S_g = -\frac{1}{4\pi p^2} \mathcal{F}_g' - \frac{C_F N_f}{N_c} S_q \quad (3.16)$$

$$\dot{F} = -\frac{C_F}{N_c} \frac{1}{p^2} (p^2 J_q)' + \frac{C_F^2}{N_c} S_q = -\frac{C_F}{N_c} \frac{1}{4\pi p^2} \mathcal{F}_q' + \frac{C_F^2}{N_c} S_q, \quad (3.17)$$

where the overdots and primes denote derivatives with respect to τ and p respectively. In these equations, the rescaled currents J_g and J_q with corresponding fluxes \mathcal{F}_g and \mathcal{F}_q have been introduced such that

$$\frac{\mathcal{F}_g}{4\pi p^2} \equiv J_g = -I_a f' - I_b f(1+f) \quad (3.18)$$

$$\frac{\mathcal{F}_q}{4\pi p^2} \equiv J_q = -I_a F' - I_b F(1-F). \quad (3.19)$$

The source terms are also rescaled as

$$S_g = -S_q = \frac{I_c}{p} [F(1+f) - f(1-F)]. \quad (3.20)$$

In these equations, the integrals I_a , I_b , and I_c are given as

$$I_a = 2\pi^2 \mathcal{I}_a = \int_0^\infty dp p^2 [N_c f(1+f) + N_f F(1-F)] \quad (3.21)$$

$$I_b = 2\pi^2 \mathcal{I}_b = 2 \int_0^\infty dp p (N_c f + N_f F) \quad (3.22)$$

$$I_c = 2\pi^2 \mathcal{I}_c = \int_0^\infty dp p (f + F). \quad (3.23)$$

Parton number density n , and energy density ϵ , can now be defined in terms of the distribution functions f and F as

$$n = 4N_c \int \frac{d^3 \mathbf{p}}{(2\pi)^3} (C_F f + N_f F) \equiv n_g + n_q \quad (3.24)$$

$$\epsilon = 4N_c \int \frac{d^3 \mathbf{p}}{(2\pi)^3} p (C_F f + N_f F) \equiv \epsilon_g + \epsilon_q. \quad (3.25)$$

The entropy density of both gluons s_g and quarks s_q can also be defined in terms of f and F as

$$s_g \equiv -4N_c C_F \int \frac{d^3 \mathbf{p}}{(2\pi)^3} [f \log f - (1+f) \log(1-f)] \quad (3.26)$$

$$s_q \equiv -4N_c C_F \int \frac{d^3 \mathbf{p}}{(2\pi)^3} [F \log F + (1-F) \log(1-F)] \quad (3.27)$$

where the total entropy density of the system is given by $s = s_g + s_q$. Taking the derivatives of n , ϵ , and s with respect to time yields the time evolution of these quantities given by

$$\dot{n} = -\frac{1}{2\pi^3} C_F (N_c \mathcal{F} + g + N_f \mathcal{F}_q) \Big|_{p=0}^{p=\infty} \quad (3.28)$$

$$\dot{\epsilon} = -\frac{1}{2\pi^3} C_F [p(N_c \mathcal{F}_g + N_f \mathcal{F}_q) + I_a 4\pi p^2 (N_c f + N_f F)] \Big|_{p=0}^{p=\infty} \quad (3.29)$$

$$\begin{aligned} \dot{s} = & \frac{C_F}{2\pi^3} \left[N_c \left(\mathcal{F}_g \log \frac{f}{1+f} - 4\pi p^2 I_b f \right) + N_f \left(\mathcal{F} \log \frac{F}{1-F} - 4\pi p^2 I_b F \right) \right] \Big|_{p=0}^{p=\infty} \\ & + \frac{2C_F}{\pi^2} \int_0^\infty dp p s^+(p), \end{aligned} \quad (3.30)$$

where $s^+(p)$ is the non-negative function

$$s^+(p) \equiv \frac{p}{I_a} \left(\frac{N_c J_g^2}{f(1+f)} + \frac{N_f J_q^2}{F(1-F)} \right) + C_F N_f I_c [F(1+f) - f(1-F)] \log \frac{F(1+f)}{f(1-F)}. \quad (3.31)$$

Following the procedure in [31], the slight temperature dependence of \mathcal{L} is neglected. This allows for equations 3.16 and 3.17 to be invariant under the scaling transformation

$$Q_s \rightarrow c Q_s, \quad \tau \rightarrow \frac{\tau}{c}, \quad \mathbf{p} \rightarrow c \mathbf{p}. \quad (3.32)$$

Therefore, the chemical potential μ , temperature T , and all momenta can be expressed in units of Q_s and time in units of $1/Q_s$.

3.3 THERMODYNAMICS OF QUARK-GLUON PLASMA

As only $2 \leftrightarrow 2$ processes are included in the collision term of the transport equations, this conserves the total parton number implying that in equilibrium, gluons and quarks/anti-quarks have the same chemical potential. The solutions to equations 3.16 and 3.17 are the thermal equilibrium distributions of the form

$$f_{eq} = \frac{1}{e^{(p-\mu)/T} - 1}, \quad F_{eq} = \frac{1}{e^{(p-\mu)/T} + 1} \quad (3.33)$$

where T and μ are the temperature and chemical potential respectively.

The QGP can be described in terms of its thermodynamic properties which are determined by the total energy density ϵ_0 and the total parton number density n_0 . In an under-populated system, solving the equations

$$\epsilon_{eq} = \epsilon_0, \quad n_{eq} = n_0 \quad (3.34)$$

can yield the values of T and $\mu < 0$, where the values of ϵ_{eq} and n_{eq} can be obtained by inserting f_{eq} and F_{eq} into equations 3.24 and 3.25. In contrast, an over-populated system has a value of n_0 so large that there is no real solution to the above equations. The thermal distribution functions, f_{eq} and F_{eq} , are found with $\mu = 0$ and a temperature determined from ϵ_0 ,

$$T = \sqrt{\frac{2}{\pi}} \frac{(15\epsilon_0)^{1/4}}{(8N_c C_F + 7N_c N_f)^{1/4}} \quad (3.35)$$

which reduces to equation A.20 if $N_f, N_c = 3$. Using equation 3.24, n_{eq} , the total number of partons with $p > 0$, can be calculated. The number density of the condensed gluons is determined using

$$N^0 = n_0 - n_{eq}, \quad (3.36)$$

and a Bose-Einstein condensate (BEC) may form from excess gluons.

3.4 TOWARD A THERMAL QGP

In [19], three different patterns of thermalization are studied. In the first case, a BEC is formed when $f_0 > f_{0c}$. In the second case, there is no BEC in the equilibrium state when $f_0 < f_{0c}$, where f_{0c} denotes the transition from under to over-population. However, when quarks are present in the case of $f_0 < f_{0c}$, a BEC may appear for a short time which is caused by the over-population of low momentum gluons. In this thesis, however, only the path to thermalization is explored. The exact means of thermalization is still the subject of much research.

Using the diffusion approximation of the Boltzmann equation, two coupled transport equations for the gluon distribution f and the quark distribution F have been derived. These transport equations are solved numerically to study how the system evolves from an initial gluon distribution given by

$$f(0, p) = f_0 \theta\left(1 - \frac{p}{Q_s}\right), \quad (3.37)$$

which is inspired by the colour glass picture [31], to the thermalized state of quark-gluon plasma.

To do this, code was developed which outputs these distributions, f and F , as a function of momentum and time such that $f = f_g(p_\perp, p_z, \tau)$ and $F = f_q(p_\perp, p_z, \tau)$. Starting with $\tau_0 = 1/Q_s$ and running until $\tau = 25/Q_s$, this code is used to study the evolution of the quark and gluon distribution functions throughout the process of thermalization. Additionally, the energy density for every timestep is also given. From this, the temperature as a function of τ , $T(\tau)$, can be calculated (see appendix A). With these distribution functions, the pre-equilibrium production rate of dileptons and photons can be determined and compared to that of the thermal case using the temperature calculated from the well defined energy density, which is the focus of this thesis.

Part III

CALCULATION OF THE PRODUCTION RATE AND YIELD OF DILEPTONS AND PHOTONS IN QGP

Now that the background information for this thesis has been presented, this section is dedicated to specific calculations of dilepton and photon production rates and yields. The production rates and yields were calculated for the pre-equilibrium case and compared to the well-known thermal equilibrium case, which has also been derived in this thesis to ensure an accurate comparison.

DILEPTON PRODUCTION IN THERMAL EQUILIBRIUM AND PRE-EQUILIBRIUM QGP

A dense system of quarks and gluons known as quark-gluon plasma forms after the relativistic collision of heavy ions which cannot be studied directly as it is very short lived. However, probes such as pairs of leptons, referred to as dileptons, can be used as a means of investigating the underlying physics as they are produced in both thermal and pre-equilibrium QGP.

This chapter starts by deriving the pre-equilibrium dilepton production rate in terms of both dR/d^4Q as well as dR/dM^2 . The dilepton production rate in thermal equilibrium is then derived and compared to the pre-equilibrium case.

4.1 DILEPTON PRODUCTION RATE IN PRE-EQUILIBRIUM QGP

Discussed in Chapter 2, relativistic kinetic theory gives the rate of production of colliding particles. This rate is known as the collision term and is the right-hand side of the Boltzmann equation. In the case of $q\bar{q} \rightarrow l^+l^-$ (figure 4), where dileptons are produced through quark/anti-quark annihilation, the rate at which this occurs can be derived starting with

$$\frac{dR}{d^4Q} = \int \frac{d^3\mathbf{p}_1}{(2\pi)^3} \frac{d^3\mathbf{p}_2}{(2\pi)^3} f(\mathbf{p}_1) f(\mathbf{p}_2) v_{q\bar{q}} \sigma_{q\bar{q}}(M) \delta^{(4)}(Q - P_1 - P_2), \quad (4.1)$$

which is the number of dileptons produced per space-time volume and four dimensional momentum-space volume. In this equation, the relativistic relative velocity is

$$v_{q\bar{q}} = \frac{\sqrt{(p_1 \cdot p_2)^2 - m_q^4}}{E_1 E_2} = \frac{M^2}{2} \quad (4.2)$$

and the total cross section is given by

$$\sigma_{q\bar{q}} = F_q \tilde{\sigma}(M) \quad (4.3)$$

where

$$F_q = \left[N_c (2s + 1)^2 \sum_f e_f^2 \right] \quad (4.4)$$

$$\tilde{\sigma}(M) = \frac{4\pi \alpha_{EM}^2}{3 M^2} \left(1 + \frac{2m_l^2}{M^2} \right) \left(1 - \frac{4m_l^2}{M^2} \right)^{1/2}. \quad (4.5)$$

Thus,

$$\sigma_{q\bar{q}} = \frac{80\pi \alpha_{EM}^2}{9 M^2} \quad (4.6)$$

where, for the purposes of this derivation, only u and d massless quarks are used and it is assumed that the rest mass of the leptons is much less than M , which is the centre-of-mass energy and the dilepton invariant mass. As this is the pre-equilibrium case, thermal distribution functions cannot be used. Therefore, the distribution functions must come from the out-of-equilibrium solution to the Boltzmann equation (see Chapter 3), where the resulting distribution functions are given in terms of p_\perp , p_z , and τ . The rate can therefore be written as

$$\frac{dR}{d^4Q} = \frac{5\alpha_{EM}^2}{72\pi^5} \int \frac{d^3\mathbf{p}_1}{E_1} \frac{d^3\mathbf{p}_2}{E_2} f_q(p_{1\perp}, p_{1z}, \tau) f_{\bar{q}}(p_{2\perp}, p_{2z}, \tau) \delta^{(4)}(P_1 + P_2 - Q). \quad (4.7)$$

Knowing that four-vectors can be expanded in terms of energy and momentum, the $\delta^{(4)}$ function can be rewritten as $\delta^{(4)}(P_1 + P_2 - Q) = \delta^{(3)}(\mathbf{p}_1 + \mathbf{p}_2 - \mathbf{Q}) \delta(E_1 + E_2 - E)$. After inserting this and integrating over \mathbf{p}_2 , the equation becomes

$$\frac{dR}{d^4Q} = \frac{5\alpha_{EM}^2}{72\pi^5} \int \frac{d^3\mathbf{p}_1}{E_1 E_2} f_q(p_{1\perp}, p_{1z}, \tau) f_{\bar{q}}(p_{2\perp}^-, p_{2z}^-, \tau) \delta(E_1 + E_2 - E). \quad (4.8)$$

In the above equation, new variables are introduced and defined as

$p_{2\perp}^- = \sqrt{Q_\perp^2 + p_{1\perp}^2 - 2Q_\perp p_{1\perp} \cos \phi_1}$ and $p_{2z}^- = Q_z - p_{1z}$, such that the integral is no longer dependent on \mathbf{p}_2 .

In order to integrate over the final delta function, the Jacobian must first be determined. Using the equation

$$\mathcal{J} = \delta(\phi_1 - \bar{\phi}_1) \frac{1}{\left| \frac{\partial g}{\partial \phi_1} \right|} = \delta(\phi_1 - \bar{\phi}_1) \frac{1}{\left| \frac{\partial g}{\partial p_{2\perp}^-} \frac{\partial p_{2\perp}^-}{\partial \phi_1} \right|}, \quad (4.9)$$

where g is the argument inside the function, the Jacobian can be calculated by rewriting the delta function in terms of the variables $p_{2\perp}$ and p_{2z}

$$\delta(g) = \delta(E_1 + E_2 - E) = \delta\left(E - E_1 - \sqrt{p_{2\perp}^2 + m_q^2 + p_{2z}^2}\right), \quad (4.10)$$

In doing so, the Jacobian is given by

$$\mathcal{J} = \delta(\phi_1 - \bar{\phi}_1) \frac{E_2}{Q_{\perp} p_{1\perp} |\sin \phi_1|}. \quad (4.11)$$

which is then used to rewrite the rate

$$\frac{dR}{d^4Q} = \frac{5\alpha_{EM}^2}{72\pi^5} \int \frac{d^3\mathbf{p}_1}{E_1 E_2} f_q(p_{1\perp}, p_{1z}, \tau) f_{\bar{q}}(p_{2\perp}, p_{2z}, \tau) \delta(\phi_1 - \bar{\phi}_1) \frac{E_2}{Q_{\perp} p_{1\perp} |\sin \phi_1|}. \quad (4.12)$$

Recalling that the integration measure can be expanded as $d^3\mathbf{p}_1 = p_{1\perp} dp_{1\perp} dp_{1z} d\phi_1$, an integration over ϕ_1 can then be performed yielding

$$\frac{dR}{d^4Q} = \frac{5\alpha_{EM}^2}{72\pi^5} \int dp_{1\perp} dp_{1z} \frac{1}{E_1 Q_{\perp}} \frac{1}{|\sin \bar{\phi}_1|} f_q(p_{1\perp}, p_{1z}, \tau) f_{\bar{q}}(p_{2\perp}, p_{2z}, \tau). \quad (4.13)$$

However, $|\sin \bar{\phi}_1|$ still needs to be determined. This can be done using the argument of the energy delta function. In this case, the energy E_2 is expressed in terms of the variables $p_{2\perp}$ and p_{2z} , giving $E - E_1 = E_2 = \sqrt{p_{2\perp}^2 + m_q^2 + p_{2z}^2}$, which can be used to determine an expression containing a factor of $\cos \bar{\phi}_1$. After squaring both sides of the equation and expanding, the expression

$$E^2 + E_1^2 - 2EE_1 = Q_{\perp}^2 + p_{1\perp}^2 - 2Q_{\perp} p_{1\perp} \cos \bar{\phi}_1 + Q_z^2 + p_{1z}^2 - 2Q_z p_{1z} + m_q^2 \quad (4.14)$$

is obtained, which can be simplified using the invariant mass equations $E_1^2 = p_{1\perp}^2 + p_{1z}^2 + m_q^2$ and $E^2 = Q_{\perp}^2 + Q_z^2 + M^2$ and rearranged such that $\cos \bar{\phi}_1$ is isolated

$$\cos \bar{\phi}_1 = \frac{2EE_1 - M^2 - 2Q_z p_{1z}}{2Q_{\perp} p_{1\perp}}. \quad (4.15)$$

Recalling the basic trigonometric identity $\sin \bar{\phi}_1 = \sqrt{1 - \cos^2 \bar{\phi}_1}$, an expression for $\sin \bar{\phi}_1$ is finally obtained

$$\sin \bar{\phi}_1 = \frac{\sqrt{4Q_{\perp}^2 p_{1\perp}^2 - (2EE_1 - M^2 - 2Q_z p_{1z})^2}}{2Q_{\perp} p_{1\perp}}. \quad (4.16)$$

Returning to the integral, the pre-equilibrium dilepton production rate can be written as

$$\begin{aligned} \frac{dR}{d^4Q} = & \frac{5\alpha_{EM}^2}{72\pi^5} \int dp_{1\perp} dp_{1z} \frac{2p_{1\perp}}{E_1} \frac{1}{\sqrt{4Q_{\perp}^2 p_{1\perp}^2 - (2EE_1 - M^2 - 2Q_z p_{1z})^2}} f_q(p_{1\perp}, p_{1z}, \tau) \\ & \times f_{\bar{q}}(\sqrt{Q_{\perp}^2 + p_{1\perp}^2 - (2EE_1 - M^2 - 2Q_z p_{1z})}, Q_z - p_{1z}, \tau). \end{aligned} \quad (4.17)$$

However, this can once again be rewritten using the known identities

$$E = \sqrt{M^2 + Q_{\perp}^2 + Q_z^2} = \sqrt{M^2 + Q_{\perp}^2} \cosh(y) \quad (4.18)$$

and

$$Q_z = \sqrt{M^2 + Q_{\perp}^2} \sinh(y). \quad (4.19)$$

In the case of boost-invariance, meaning that the system remains unchanged if a Lorentz transformation is applied, the rapidity may be set to $y = 0$. Thus, the identities simplify to

$$E = \sqrt{M^2 + Q_{\perp}^2} \quad (4.20)$$

$$Q_z = 0. \quad (4.21)$$

Therefore, the final expression for the pre-equilibrium dilepton production rate becomes

$$\begin{aligned} \frac{dR}{d^4Q} = & \frac{5\alpha_{EM}^2}{72\pi^5} \int dp_{1\perp} dp_{1z} \frac{2p_{1\perp}}{E_1} \frac{1}{\sqrt{4Q_{\perp}^2 p_{1\perp}^2 - (2EE_1 - M^2)^2}} f_q(p_{1\perp}, p_{1z}, \tau) \\ & \times f_{\bar{q}}(\sqrt{Q_{\perp}^2 + p_{1\perp}^2 - (2EE_1 - M^2)}, -p_{1z}, \tau). \end{aligned} \quad (4.22)$$

Now the limits of integration need to be determined. For p_{1z} , the integration limits can be determined from $\cos \bar{\phi}_1$ as

$$\cos \bar{\phi}_1 = \left| \frac{2EE_1 - M^2 - 2Q_z p_{1z}}{2Q_{\perp} p_{1\perp}} \right| \leq 1. \quad (4.23)$$

Taking the argument of the cosine to be negative, possible limits of integration for p_{1z} are given by

$$\frac{-b_1 - \sqrt{b_1^2 - 4a_1 c_1}}{2a_1} \leq p_{1z} \leq \frac{-b_1 + \sqrt{b_1^2 - 4a_1 c_1}}{2a_1}. \quad (4.24)$$

where

$$a_1 = 4(E^2 - Q_z^2) \quad (4.25)$$

$$b_1 = -4Q_z(M^2 - 2Q_\perp p_{1\perp}) \quad (4.26)$$

$$c_1 = -(M^2 - 2Q_\perp p_{1\perp})^2 + 4E^2 p_{1\perp}^2 + 4E^2 m_q^2. \quad (4.27)$$

However, taking the argument of the cosine to be positive yields the limits

$$\frac{-b_2 - \sqrt{b_2^2 - 4a_2 c_2}}{2a_2} \leq p_{1z} \leq \frac{-b_2 + \sqrt{b_2^2 - 4a_2 c_2}}{2a_2} \quad (4.28)$$

where

$$a_2 = 4(E^2 - Q_z^2) \quad (4.29)$$

$$b_2 = -4Q_z(M^2 + 2Q_\perp p_{1\perp}) \quad (4.30)$$

$$c_2 = -(M^2 + 2Q_\perp p_{1\perp})^2 + 4E^2 p_{1\perp}^2 + 4E^2 m_q^2. \quad (4.31)$$

The limits of integration for $p_{1\perp}$ come from

$$p_{1\perp}^2 = \sqrt{Q_\perp^2 + p_{1\perp}^2 - (2EE_1 - M^2)}, \quad (4.32)$$

such that the argument under the square root must be greater than zero. After some algebraic manipulation, this equation becomes

$$p_{1\perp} \leq \sqrt{E^2 - Em_q}. \quad (4.33)$$

Therefore, for massless quarks, the limits of $p_{1\perp}$ are

$$0 \leq p_{1\perp} \leq E. \quad (4.34)$$

The pre-equilibrium dilepton production rate can also be written in terms of mass distribution knowing that

$$\frac{dR}{d^4Q} = \frac{dR}{MdMdyd^2Q_\perp}, \quad (4.35)$$

where, $MdM = \frac{1}{2}dM^2$ and, as before, $y = 0$. Therefore, by integrating over Q_\perp , an alternate expression for the rate is given by

$$\begin{aligned} \frac{dR}{dM^2} = \frac{5\alpha_{EM}^2}{72\pi^5} \int dp_{1\perp} dp_{1z} dQ_\perp \frac{2p_{1\perp}}{E_1} \frac{Q_\perp}{\sqrt{4Q_\perp^2 p_{1\perp}^2 - (2EE_1 - M^2)^2}} f_q(p_{1\perp}, p_{1z}, \tau) \\ \times f_{\bar{q}}(\sqrt{Q_\perp^2 + p_{1\perp}^2 - (2EE_1 - M^2)}, -p_{1z}, \tau). \end{aligned} \quad (4.36)$$

4.2 DILEPTON PRODUCTION RATE IN THERMAL QGP

Starting with the same equation as before,

$$\frac{dR}{d^4Q} = \int \frac{d^3\mathbf{p}_1}{(2\pi)^3} \frac{d^3\mathbf{p}_2}{(2\pi)^3} f(\mathbf{p}_1) f(\mathbf{p}_2) v_{q\bar{q}} \sigma_{q\bar{q}} \delta^{(4)}(Q - P_1 - P_2), \quad (4.37)$$

the dilepton production rate can be determined for the case when the quark-gluon plasma is in thermal equilibrium. In this case, Maxwell-Boltzmann statistics are used for the thermal distribution functions such that

$$f(\mathbf{p}_1) f(\mathbf{p}_2) = e^{-(E_1+E_2)/T} = e^{-E/T} = e^{-\beta E}. \quad (4.38)$$

After the distribution functions, cross-section $\sigma_{q\bar{q}}$, and the expression $v_{q\bar{q}}$ have been inserted, the rate equation is given by

$$\frac{dR}{d^4Q} = \frac{40\pi}{9} \alpha_{EM}^2 \int \frac{d^3\mathbf{p}_1 d^3\mathbf{p}_2}{(2\pi)^6 E_1 E_2} e^{-\beta E} \delta^{(4)}(Q - P_1 - P_2). \quad (4.39)$$

Knowing that the $\delta^{(4)}$ function can be expanded into it's energy and momentum components,

$$\frac{dR}{d^4Q} = \frac{40\pi}{9} \alpha_{EM}^2 \int \frac{d^3\mathbf{p}_1 d^3\mathbf{p}_2}{(2\pi)^6 E_1 E_2} e^{-\beta E} \delta(E - E_1 - E_2) \delta^{(3)}(\mathbf{Q} - \mathbf{p}_1 - \mathbf{p}_2), \quad (4.40)$$

From the three-momentum delta function, is it known that $\mathbf{p}_2 = \mathbf{Q} - \mathbf{p}_1$. Therefore, the energy delta function can be rewritten knowing that

$$E_2 = E - E_1 = |\mathbf{p}_2| = \sqrt{\mathbf{Q}^2 + \mathbf{p}_1^2 - 2|\mathbf{Q}||\mathbf{p}_1| \cos \theta} \quad (4.41)$$

After integrating over \mathbf{p}_2 , the above expression is substituted into the energy delta function yielding

$$\frac{dR}{d^4Q} = \frac{40\pi}{9} \alpha_{EM}^2 \int \frac{|\mathbf{p}_1|^2 d\mathbf{p}_1 dz d\phi}{(2\pi)^6 E_1 (E - E_1)} e^{-\beta E} \delta\left(E - E_1 - \sqrt{\mathbf{Q}^2 + \mathbf{p}_1^2 - 2|\mathbf{Q}||\mathbf{p}_1|z}\right), \quad (4.42)$$

where d^3p_1 has been as $|p_1|^2 dp_1 dz d\phi$ and dz is the angular dependence such that $\cos \theta = z$. Now the Jacobian from the energy delta function must be determined. This can be computed using the equation

$$\mathcal{J} = \frac{\delta(z - z_0)}{f'(z_0)}, \quad (4.43)$$

which gives a Jacobian of

$$\mathcal{J} = \frac{E - E_1}{2|\mathbf{Q}|E_1}. \quad (4.44)$$

Therefore, after integrating over ϕ , which gives a factor of 2π , z can also be integrated over which gives

$$\frac{dR}{d^4Q} = \frac{80\pi^2}{9}\alpha_{EM}^2 \int \frac{d\mathbf{p}_1}{(2\pi)^6} \frac{e^{-\beta E}}{2|\mathbf{Q}|}. \quad (4.45)$$

In order to complete the last integral over \mathbf{p}_1 , the limits of integration must be determined. This can be done from the energy delta function where

$$E - E_1 = \sqrt{\mathbf{Q}^2 + \mathbf{p}_1^2 - 2|\mathbf{Q}||\mathbf{p}_1|z}. \quad (4.46)$$

After expanding this expression and isolating for p_1

$$p_1 = \frac{E^2 - \mathbf{Q}^2}{2(E \mp |\mathbf{Q}|)}, \quad (4.47)$$

the limits of integration are therefore given as

$$\frac{E^2 - \mathbf{Q}^2}{2(E + |\mathbf{Q}|)} < p_1 < \frac{E^2 - \mathbf{Q}^2}{2(E - |\mathbf{Q}|)}. \quad (4.48)$$

Performing this integration, the final expression for the thermal dilepton production rate is given by

$$\frac{dR}{d^4Q} = \frac{5\alpha_{EM}^2 e^{-\beta E}}{72\pi^4}. \quad (4.49)$$

Alternatively, as in the case of [21], the thermal dilepton production rate can be written in terms of its invariant mass distribution by inserting a delta function

$$\frac{dR}{dM^2} = \int \frac{d^3\mathbf{p}_1 d^3\mathbf{p}_2}{(2\pi)^3(2\pi)^3} \sigma(M) f(\mathbf{p}_1) f(\mathbf{p}_2) \frac{\sqrt{(P_1 \cdot P_2)^2 - m_a^4}}{E_1 E_2} \delta(M^2 - (P_1 + P_2)^2) \quad (4.50)$$

where m_a denotes the rest mass of quarks/anti-quarks. Using the Maxwell-Boltzmann statistics or the particle distribution functions as before, $f(\mathbf{p}_1) f(\mathbf{p}_2) \rightarrow e^{-\beta(E_1 + E_2)}$, the rate becomes

$$\frac{dR}{dM^2} = \int \frac{d^3\mathbf{p}_1 d^3\mathbf{p}_2}{(2\pi)^6} \sigma(M) \frac{\sqrt{(P_1 \cdot P_2)^2 - m_a^4}}{E_1 E_2} e^{-\beta(E_1 + E_2)} \delta(M^2 - (P_1 + P_2)^2). \quad (4.51)$$

The differential reaction rate can be rewritten using $P_1 \cdot P_2 = E_1 E_2 - p_1 p_2 z$ and $(P_1 + P_2)^2 = 2m_a^2 + 2(E_1 E_2 - |\mathbf{p}_1||\mathbf{p}_2|z)$. Therefore, the equation becomes

$$\frac{dR}{dM^2} = \frac{\sigma(M)}{(2\pi)^6} \int d^3\mathbf{p}_1 d^3\mathbf{p}_2 e^{-\beta(E_1+E_2)} \frac{\sqrt{(E_1 E_2 - |\mathbf{p}_1||\mathbf{p}_2|z)^2 - m_a^4}}{E_1 E_2} \times \delta(M^2 - 2m_a^2 - 2E_1 E_2 + 2|\mathbf{p}_1||\mathbf{p}_2|z). \quad (4.52)$$

Expanding the integration measures as $d^3\mathbf{p}_1 = |\mathbf{p}_1|^2 d\mathbf{p}_1 d\Omega$ and $d^3\mathbf{p}_2 = |\mathbf{p}_2|^2 d\mathbf{p}_2 dz d\phi$ and integrating over $d\phi$ and $d\Omega$ gives

$$\frac{dR}{dM^2} = \frac{(2\pi)(4\pi)}{(2\pi)^6} \sigma(M) \int |\mathbf{p}_1|^2 d\mathbf{p}_1 |\mathbf{p}_2|^2 d\mathbf{p}_2 dz \frac{\sqrt{(E_1 E_2 - |\mathbf{p}_1||\mathbf{p}_2|z)^2 - m_a^4}}{E_1 E_2} \times e^{-\beta(E_1+E_2)} \delta(M^2 - 2m_a^2 - 2E_1 E_2 + 2|\mathbf{p}_1||\mathbf{p}_2|z) \quad (4.53)$$

where the delta function can be rewritten in terms of z and $z_0 = \frac{2E_1 E_2 + 2m_a^2 - M^2}{2|\mathbf{p}_1||\mathbf{p}_2|}$ which yields a Jacobian of $\mathcal{J} = \frac{1}{2|\mathbf{p}_1||\mathbf{p}_2|}$ such that the equation becomes

$$\frac{dR}{dM^2} = \frac{(2\pi)(4\pi)}{(2\pi)^6} \sigma(M) \int |\mathbf{p}_1|^2 d\mathbf{p}_1 |\mathbf{p}_2|^2 d\mathbf{p}_2 dz \frac{\sqrt{(E_1 E_2 - |\mathbf{p}_1||\mathbf{p}_2|z)^2 - m_a^4}}{E_1 E_2} \times e^{-\beta(E_1+E_2)} \frac{\delta(z - z_0)}{2|\mathbf{p}_1||\mathbf{p}_2|}. \quad (4.54)$$

After integrating over z , the expression can be written as

$$\frac{dR}{dM^2} = \frac{(2\pi)(4\pi)}{(2\pi)^6} \frac{\sigma(M)}{4} M \sqrt{M^2 - 4m_a^2} \int dE_1 dE_2 e^{-\beta(E_1+E_2)}. \quad (4.55)$$

where the integration variables have been converted using $pdp = EdE$. Now, define the variables $E_1 + E_2 = x$ and $E_1 - E_2 = y$, which gives a Jacobian of $\mathcal{J} = \frac{1}{2}$. Using these variables to rewrite the equation

$$\frac{dR}{dM^2} = \frac{(2\pi)(4\pi)}{(2\pi)^6} \frac{\sigma(M)}{4} \frac{M \sqrt{M^2 - 4m_a^2}}{2} \int dx dy e^{-\beta x}. \quad (4.56)$$

To compute this integral, the limits of integration must be determined. For y , the limits are determined from the delta function as $2|\mathbf{p}_1||\mathbf{p}_2| \leq 2E_1 E_2 + 2m_a^2 - M^2$. Expanding this equality and rewriting in terms of the variables x and y , the in integration limits for y are obtained

$$y \geq \pm \frac{1}{M} \sqrt{(x^2 - M^2)(M^2 - 4m_a^2)} \quad (4.57)$$

Performing the intergration over y yields

$$\frac{dR}{dM^2} = \frac{\sigma(M)}{2(2\pi)^4} (M^2 - 4m_a^2) \int_{x_{min}}^{\infty} dx e^{-\beta x} M \sqrt{\frac{x^2}{M^2} - 1}. \quad (4.58)$$

Recognizing that the integral over x is a Bessel function of the second kind, the equation becomes

$$\frac{dR}{dM^2} = \frac{\sigma(M)}{2(2\pi)^4} (M^2 - 4m_a^2) \frac{M}{\beta} K_1(\beta M). \quad (4.59)$$

After inserting the total cross-section and taking all particles to be massless, the final expression for the thermal dilepton production rate is given by

$$\frac{dR}{dM^2} = \frac{5\alpha_{EM}^2}{18\pi^3} MTK_1\left(\frac{M}{T}\right). \quad (4.60)$$

This can be converted from a differential to total rate by integrating over dM^2

$$R(T) = \int_0^\infty \frac{5\alpha_{EM}^2}{18\pi^3} MTK_1\left(\frac{M}{T}\right) dM^2 \quad (4.61)$$

$$= \int_0^\infty \frac{5\alpha_{EM}^2}{18\pi^3} MTK_1\left(\frac{M}{T}\right) 2MdM \quad (4.62)$$

Defining the variable $z = \frac{M}{T}$ where $dz = \frac{1}{T}dM$, the integral becomes

$$R(T) = \frac{10\alpha_{EM}^2}{18\pi^3} \int_0^\infty T^4 z^2 K_1(z) dz. \quad (4.63)$$

After an integration over z , the total reaction rate is given by

$$R(T) = \frac{10}{9\pi^3} \alpha_{EM}^2 T^4 \quad (4.64)$$

which agrees with the expression derived in [21].

4.3 COMPARISON BETWEEN THERMAL AND PRE-EQUILIBRIUM PRODUCTION RATES

4.3.1 Ensuring consistency

In the above derivations, it was assumed that only massless up and down quarks were used. However, in the procedure used to solve the Boltzmann equation, $N_f = 3$ was used, meaning that strange quarks were also included. The equation

$$F_q = N_c(2s + 1)^2 \sum_f e_f^2 \quad (4.65)$$

which sums over the spin and flavour of quarks yields the factor $F_q = 20/3$ for up and down quarks and $F_q = 24/3$ if strange quarks are also included, which would increase the rate by 20%. Therefore, multiplying the equations by a factor of 6/5 modifies the rates to account for the additional quark. Additionally, when using the Boltzmann equation solving procedure to obtain the pre-equilibrium distribution functions, a non-zero chemical potential was used. Thus, the thermal distribution functions must also be modified to include the chemical potential as $e^{-(E_1-\mu)\beta}e^{-(E_2-\mu)\beta} = e^{-(E_1+E_2-2\mu)\beta} = e^{-(E-2\mu)\beta}$.

With these considerations in mind, the expressions for the pre-equilibrium dilepton production rate become

$$\frac{dR}{d^4Q} = \frac{\alpha_{EM}^2}{12\pi^5} \int dp_{1\perp} dp_{1z} \frac{2p_{1\perp}}{E_1} \frac{1}{\sqrt{4Q_{\perp}^2 p_{1\perp}^2 - (2EE_1 - M^2)^2}} f_q(p_{1\perp}, p_{1z}, \tau) \times f_{\bar{q}}(\sqrt{Q_{\perp}^2 + p_{1\perp}^2 - (2EE_1 - M^2)}, -p_{1z}, \tau) \quad (4.66)$$

$$\frac{dR}{dM^2} = \frac{\alpha_{EM}^2}{12\pi^5} \int dp_{1\perp} dp_{1z} dQ_{\perp} \frac{2p_{1\perp}}{E_1} \frac{Q_{\perp}}{\sqrt{4Q_{\perp}^2 p_{1\perp}^2 - (2EE_1 - M^2)^2}} f_q(p_{1\perp}, p_{1z}, \tau) \times f_{\bar{q}}(\sqrt{Q_{\perp}^2 + p_{1\perp}^2 - (2EE_1 - M^2)}, -p_{1z}, \tau), \quad (4.67)$$

and

$$\frac{dR}{d^4Q} = \frac{\alpha_{EM}^2 e^{-(E-2\mu)/T}}{12\pi^4} \quad (4.68)$$

$$\frac{dR}{dM^2} = \frac{\alpha_{EM}^2 e^{2\mu/T}}{3\pi^3} MTK_1\left(\frac{M}{T}\right). \quad (4.69)$$

for the thermal production rate. By enforcing that the energy and number density for the pre-equilibrium (ϵ_{num}, n_{num}) are equal to the thermal case at every time step, solving the system of equations

$$\epsilon_{num} = v_g \int \frac{d^3\mathbf{p}}{(2\pi)^3} E \frac{1}{e^{(E-\mu)/T} - 1} + v_q \int \frac{d^3\mathbf{p}}{(2\pi)^3} E \frac{1}{e^{(E-\mu)/T} + 1} \quad (4.70)$$

$$n_{num} = v_g \int \frac{d^3\mathbf{p}}{(2\pi)^3} \frac{1}{e^{(E-\mu)/T} - 1} + v_q \int \frac{d^3\mathbf{p}}{(2\pi)^3} \frac{1}{e^{(E-\mu)/T} + 1} \quad (4.71)$$

numerically can determine the temperature and chemical potential as a function of time as shown in figures 6 and 7 respectively.

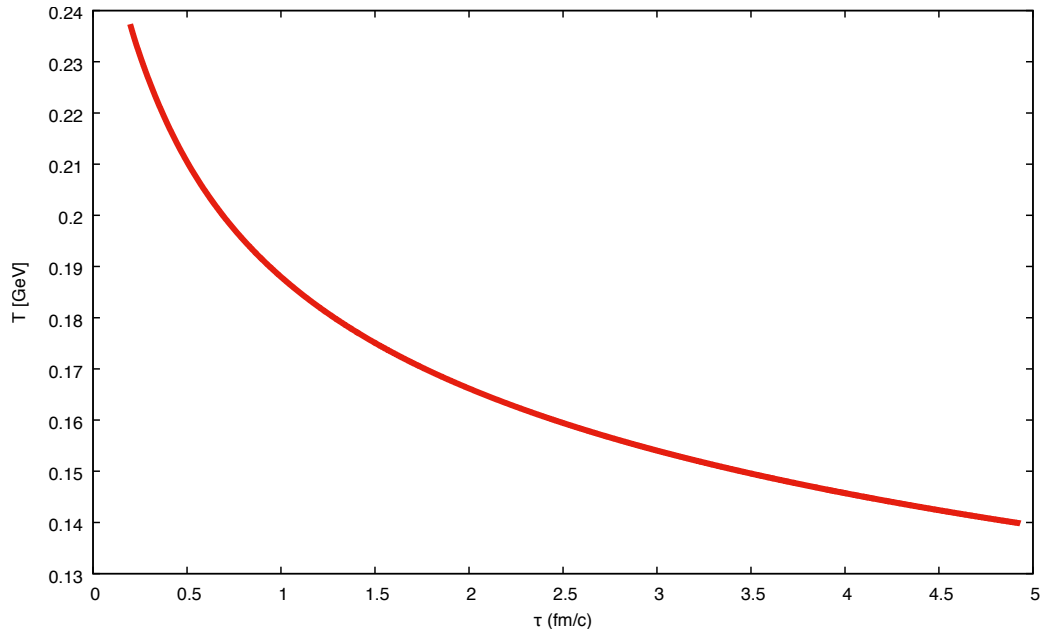


Figure 6: The temperature evolution plotted as a function of time for $Q_s = 1$ GeV.

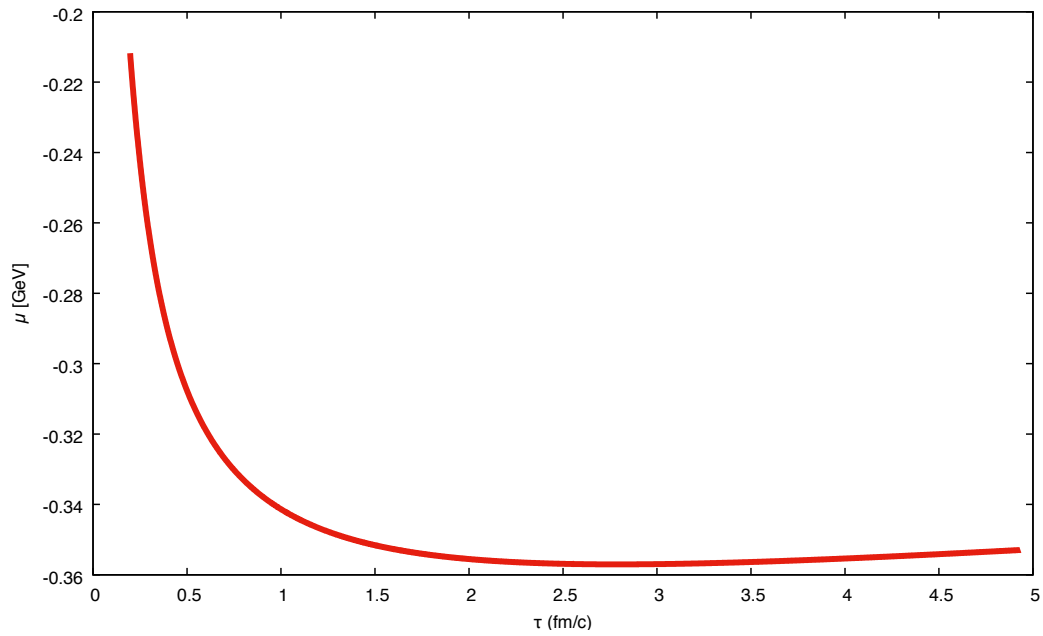


Figure 7: The chemical potential evolution plotted as a function of time for $Q_s = 1$ GeV.

4.3.2 Comparison

The pre-equilibrium system created immediately after a heavy ion collision evolves from a dense system containing mostly gluons as pairs of quarks and anti-quarks are created. For the purposes of this study, only very early times starting with an initial time given as $1/Q_s$ and evolved until $25/Q_s$ are investigated. As described in [33], the value of Q_s can range from 1-2 GeV. Thus, the values of $Q_s = 1$ GeV and $Q_s = 2$ GeV were chosen to investigate how the rate is affected. In the first case, the pre-equilibrium evolution begins with an initial temperature $T \sim 240$ MeV and studied for the duration of ~ 5 fm/c. However, as time is given in units of $1/Q_s$ and temperature is given in units of Q_s , doubling the value of Q_s to 2 GeV results in doubling the initial temperature to $T \sim 480$ MeV but decreases the evolution duration by half to ~ 2.5 fm/c.

The expression for the dilepton rate for the pre-equilibrium case, derived in the previous section, is given by equation 4.66. This equation was numerically integrated using the distribution functions calculated using the methods in [19]. Figure 8 shows the results of the numerical integration for various timesteps corresponding to different points in the evolution of the QGP. The temperatures listed were computed as described in the previous subsection. As shown, higher temperatures are generally equated with a larger production rate, especially for low transverse momentum. This is to be expected as higher temperatures mean that particles have higher energies and therefore more energy is available for particle production.

It is also interesting to note that at larger transverse momentum, the rate calculated from the highest temperature plotted dips below the rate calculated using the second highest temperature chosen since it would be expected that a higher temperature would correspond to a larger production rate. However, because the QGP starts out as a system consisting of mainly gluons, and as the higher temperature corresponds to such an early time ($2/Q_s$) in the evolution, there was insufficient time to create enough quark/anti-quark pairs to produce dileptons, especially those with large transverse momentum. The finiteness of the quark phase space, owing to their small number, becomes clear. This is evident in figure 12 which shows that the production rate is very low at times less than 0.5 fm/c when $Q_s = 1$ GeV and times less than 0.25 fm/c when $Q_s = 2$ GeV. This

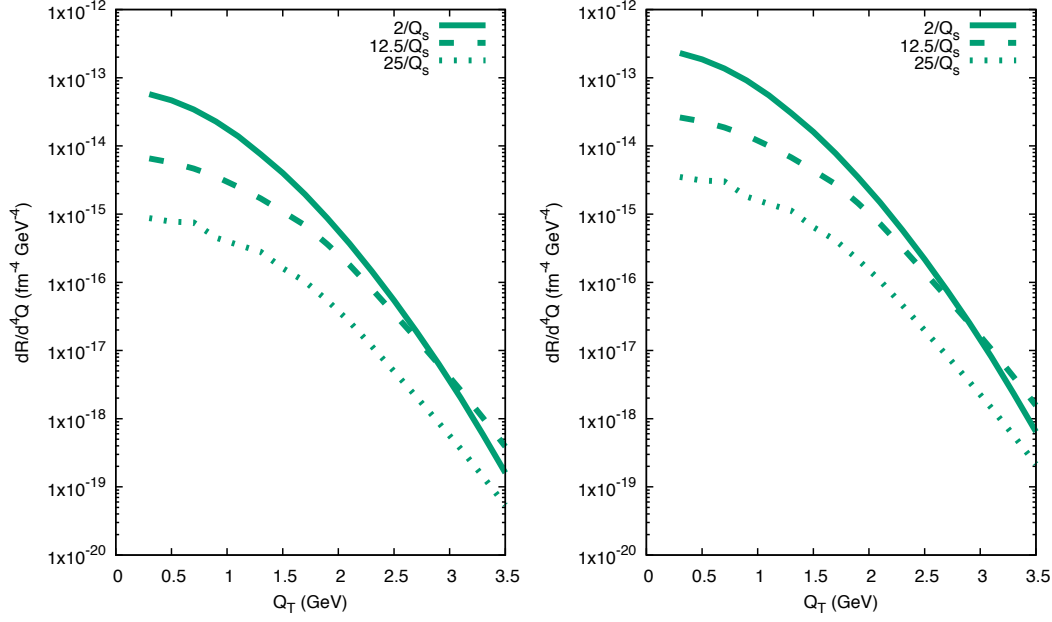


Figure 8: The pre-equilibrium dilepton production rate plotted for the timesteps $2/Q_s$, $12.5/Q_s$, and $25/Q_s$, which correspond to the temperatures 218 MeV, 160 MeV, and 140 MeV for $Q_s = 1$ GeV (left) and 436 MeV, 320 MeV, and 280 MeV for $Q_s = 2$ GeV (right). The dilepton invariant mass is set to $M = 3$ GeV in both cases.

observation is in fact one of the main findings of this work. The low fermion population makes it very difficult for the electromagnetic signal to shine.

The results for the pre-equilibrium case were compared to the known expression for the thermal equilibrium case, also derived previously, which is given by equation 4.68. In order to ensure a meaningful comparison, the temperature and chemical potential in both the thermal and pre-equilibrium cases should be equal. For the pre-equilibrium case, the timestep $2/Q_s$ was chosen which corresponds to $T = 218$ MeV, $\mu = -0.29$ GeV for $Q_s = 1$ GeV and $T = 436$ MeV, $\mu = -0.58$ GeV for $Q_s = 2$ GeV, so these values were used in the expression for the thermal rate. As shown in figure 9, the thermal dilepton production rate is about one to two orders of magnitude larger than that of the pre-equilibrium case for $Q_s = 1$ GeV and more than four orders of magnitude when $Q_s = 2$ GeV. This is due to the fact that the pre-equilibrium case is still evolving from mainly gluons towards thermal quark-gluon plasma, which is evident in figures 10 and 11 as the pre-equilibrium number densities are initially very different but asymptotically tend to the ordering of the thermal equilibrium number densities. As there are less quark/anti-

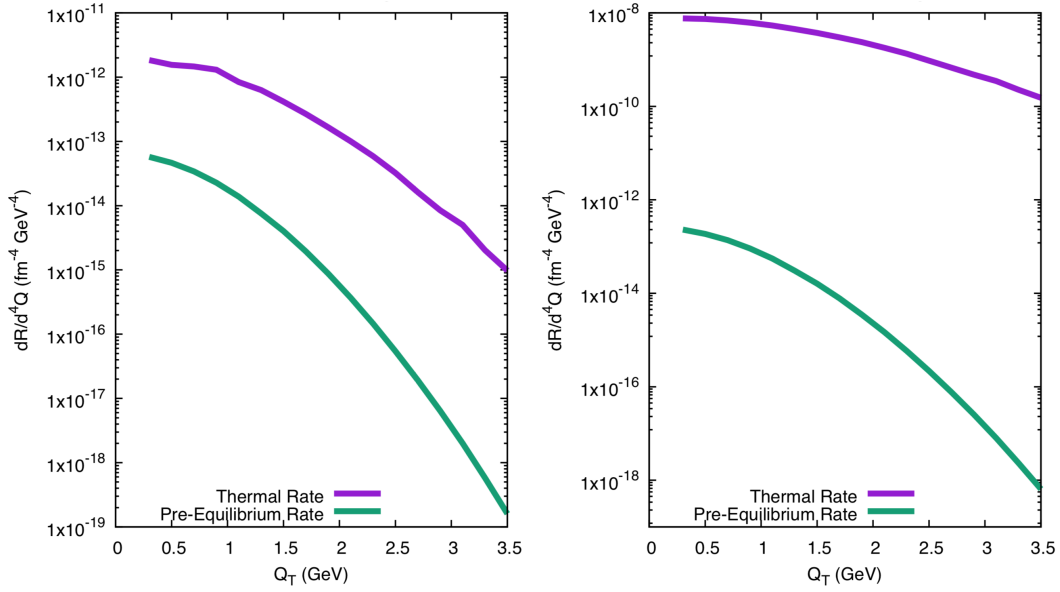


Figure 9: The dilepton production rate in thermal equilibrium is plotted and compared to the pre-equilibrium rate calculated using the timestep $2/Q_s$ which corresponds to the same temperature. For $Q_s = 1$ GeV (left), the temperature $T = 218$ MeV and $T = 436$ MeV for $Q_s = 2$ GeV (right).

quark pairs present, there are less dileptons produced from their annihilation, so the production rate is much lower.

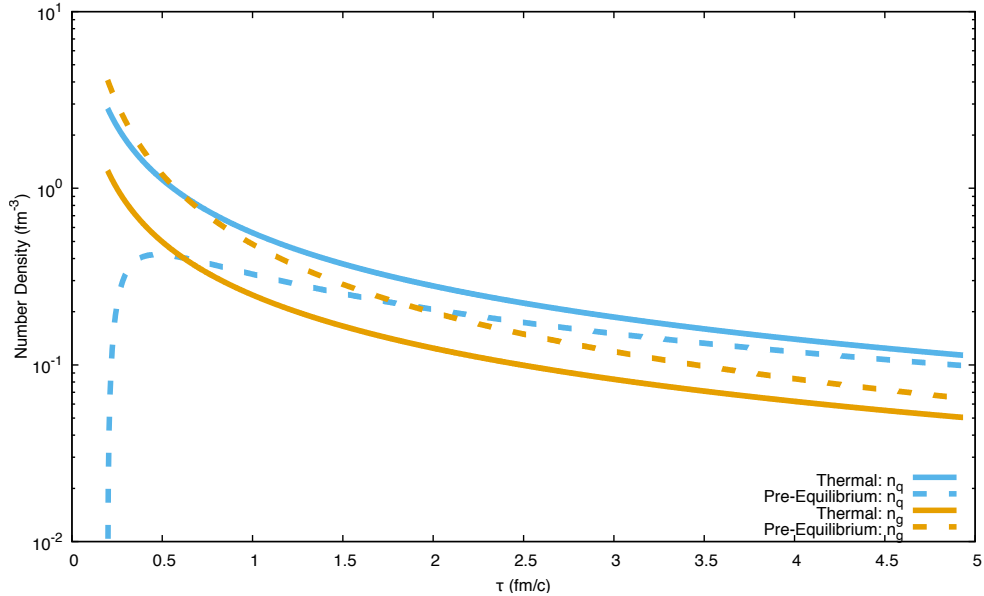


Figure 10: The number density of quarks and gluons in thermal equilibrium compared to that in the pre-equilibrium case computed using the methods described in Chapter 3 for $Q_s = 1$ GeV.

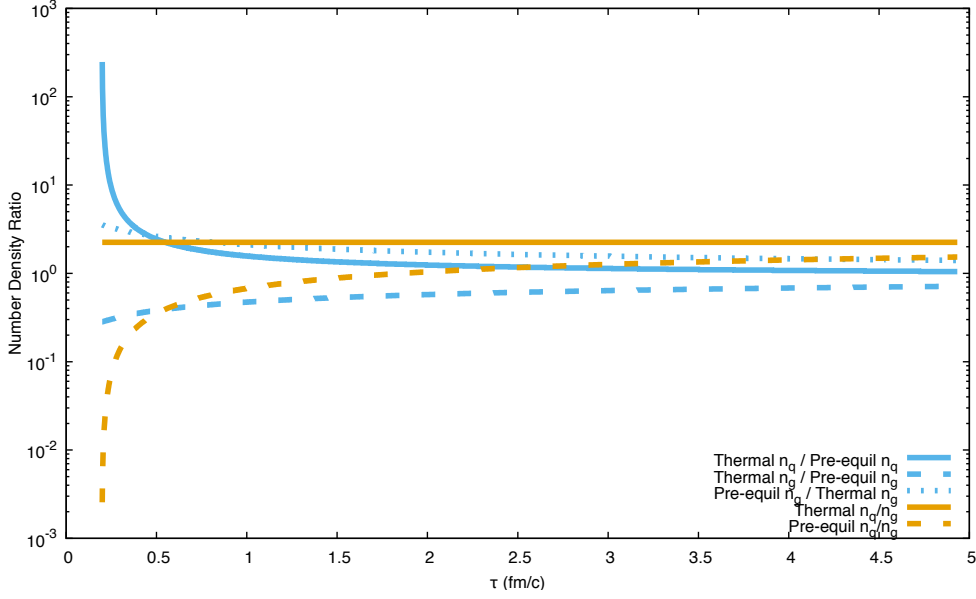


Figure 11: The ratio of the number density of thermal quarks/gluons to pre-equilibrium quarks/gluons (shown in blue) and the ratio of the number density of quarks to gluons in both the thermal and pre-equilibrium QGP (shown in orange) are compared for $Q_s = 1$ GeV.

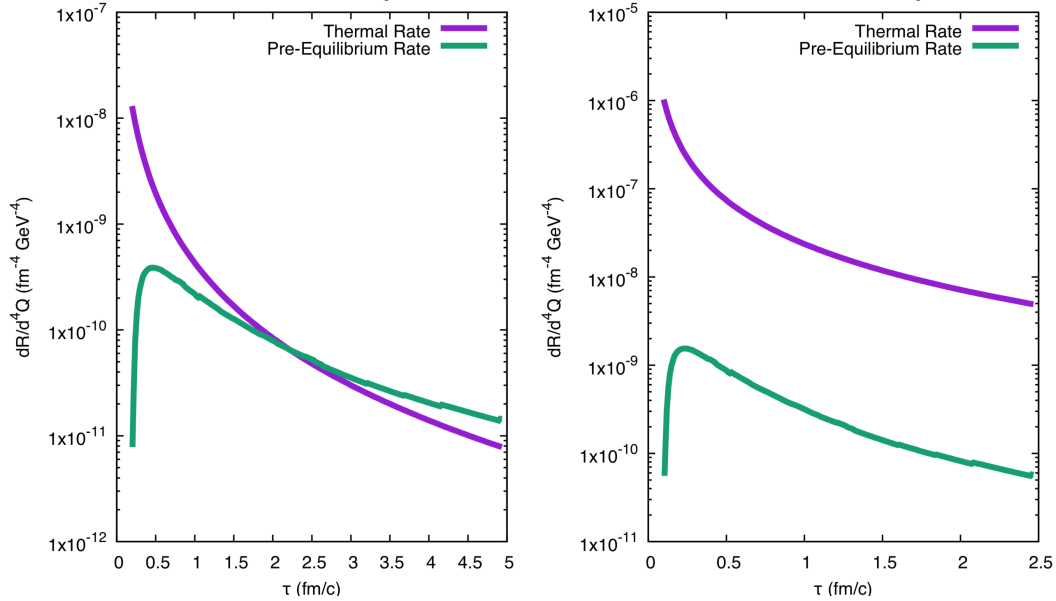


Figure 12: The dilepton production rate in thermal equilibrium is plotted and compared to the pre-equilibrium rate as a function of time for both $Q_s = 1$ GeV (left) and $Q_s = 2$ GeV (right). In this plot, the values of both Q_\perp and M are taken to be 1 GeV.

Alternatively, the production rate can be written in terms of mass distribution as in equation 4.67 for the thermal case and equation 4.69 for the pre-equilibrium case. As

before, the temperature was matched using the timestep $2/Q_s$ which corresponds to $T = 218$ MeV, $\mu = -0.29$ GeV for $Q_s = 1$ GeV and $T = 436$ MeV, $\mu = -0.58$ GeV for $Q_s = 2$ GeV to be used in the thermal case. The comparison is shown in figure 13, where it is again evident that thermal QGP has a larger dilepton production rate than the pre-equilibrium case.

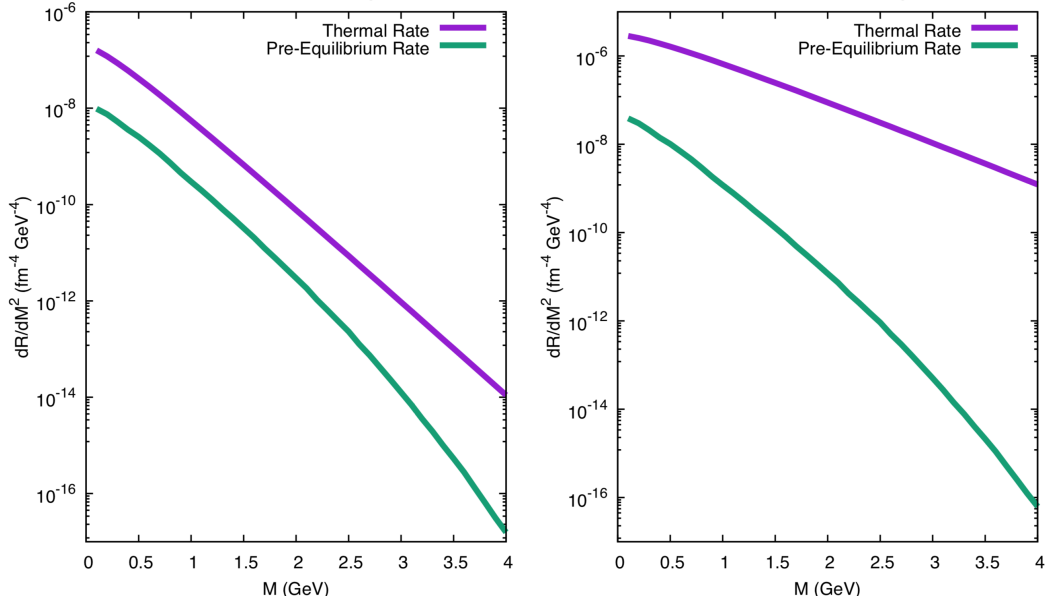


Figure 13: The dilepton production rate as a function of mass in thermal equilibrium is plotted and compared to the pre-equilibrium rate calculated using the timestep $2/Q_s$. On the left $Q_s = 1$ GeV and on the right $Q_s = 2$ GeV.

DILEPTON YIELD IN THERMAL EQUILIBRIUM AND PRE-EQUILIBRIUM QGP

In heavy ion collisions, analyzing the rate at which particles are produced can be a very useful tool for understanding how the system evolves. Experimentally, however, the rate of production cannot be directly observed. Only the actual number of particles produced, the yield, can be measured by detectors. In this section, the dilepton yield for both thermal equilibrium and pre-equilibrium cases are derived and compared.

5.1 DILEPTON YIELD IN PRE-EQUILIBRIUM QGP

As previously determined, the pre-equilibrium dilepton production rate is given by

$$\begin{aligned} \frac{dR}{dM^2} = \frac{\alpha_{EM}^2}{12\pi^5} \int dp_{1\perp} dp_{1z} dQ_{\perp} \frac{2p_{1\perp}}{E_1} \frac{Q_{\perp}}{\sqrt{4Q_{\perp}^2 p_{1\perp}^2 - (2EE_1 - M^2)^2}} f_q(p_{1\perp}, p_{1z}, \tau) \\ \times f_{\bar{q}}(\sqrt{Q_{\perp}^2 + p_{1\perp}^2 - (2EE_1 - M^2)}, -p_{1z}, \tau) \end{aligned} \quad (5.1)$$

where massless u , d , and s quarks have been taken into consideration. Now recall that rate can be expanded as

$$\frac{dR}{d^4Q} = \frac{dN}{d^4X d^4Q} = \frac{dN}{MdM dy d^2Q_{\perp} d^2x_{\perp} \tau d\tau d\eta} = \frac{dN}{\frac{1}{2} dM^2 dy d^2Q_{\perp} d^2x_{\perp} \tau d\tau d\eta} \quad (5.2)$$

where an integration over Q_{\perp} , x_{\perp} , and τ would leave only $dN/MdM dy d\eta$ on the left-hand side. Also recall that dR/d^4Q was derived for the case where $y = 0$. Therefore, the pre-equilibrium dilepton yield can be determined using

$$\frac{dN}{dM^2 d\eta} = \frac{1}{2} \int d^2Q_{\perp} d^2x_{\perp} \tau d\tau \frac{dR}{d^4Q}, \quad (5.3)$$

where $d^2Q_{\perp} = Q_{\perp} dQ_{\perp}$ and the integration over x_{\perp} is simply taken to be the overlapping area of the two colliding nuclei. For perfectly central collisions, this area is given by πR_T^2

where $R_T = 1.2A^{1/3}$ [34] is the radius of the nucleus in the transverse plane. Thus, the pre-equilibrium dilepton yield can be determined from the expression

$$\begin{aligned} \frac{dN}{dM^2 d\eta} &= \frac{1}{2} \pi R_T^2 \int \tau d\tau \frac{\alpha_{EM}^2}{12\pi^5} \int dp_{1\perp} dp_{1z} Q_{\perp} dQ_{\perp} \frac{2p_{1\perp}}{E_1} \frac{1}{\sqrt{4Q_{\perp}^2 p_{1\perp}^2 - (2EE_1 - M^2)^2}} \\ &\quad \times f_q(p_{1\perp}, p_{1z}, \tau) f_{\bar{q}}(\sqrt{Q_{\perp}^2 + p_{1\perp}^2 - (2EE_1 - M^2)}, -p_{1z}, \tau). \end{aligned} \quad (5.4)$$

The integral over τ must be converted to a summation to sum over all timesteps from $1/Q_s$ to $25/Q_s$, so the final expression for the pre-equilibrium dilepton yield becomes

$$\begin{aligned} \frac{dN}{dM^2 d\eta} &= \frac{1}{2} \pi R_T^2 \sum_i \tau_i \Delta\tau \frac{\alpha_{EM}^2}{12\pi^5} \int dp_{1\perp} dp_{1z} Q_{\perp} dQ_{\perp} \frac{2p_{1\perp}}{E_1} \frac{1}{\sqrt{4Q_{\perp}^2 p_{1\perp}^2 - (2EE_1 - M^2)^2}} \\ &\quad \times f_q(p_{1\perp}, p_{1z}, \tau) f_{\bar{q}}(\sqrt{Q_{\perp}^2 + p_{1\perp}^2 - (2EE_1 - M^2)}, -p_{1z}, \tau). \end{aligned} \quad (5.5)$$

5.2 DILEPTON YIELD IN THERMAL QGP

For thermal quark-gluon plasma, recall that the thermal dilepton production rate previously derived is given by

$$\frac{dR}{dM^2} = \frac{\alpha_{EM}^2}{3\pi^3} e^{2\mu/T} MTK_1\left(\frac{M}{T}\right) \quad (5.6)$$

where only massless u , d , and s quarks have been taken into consideration. As in the pre-equilibrium case, this rate can be expanded as $dR/dM^2 = dN/d^4X dM^2 = dN/d^2x_{\perp} \tau d\tau d\eta dM^2$. Therefore, the expression for the thermal dilepton yield can be written as

$$\frac{dN}{dM^2 d\eta} = \pi R_T^2 \int \tau d\tau \frac{\alpha_{EM}^2}{3\pi^3} e^{2\mu/T} MTK_1\left(\frac{M}{T}\right) \quad (5.7)$$

where the factor of πR_T^2 again comes from the integration over x_{\perp} . The τ integral can now be converted to a sum as the temperature is a function of τ as described in section 4.3.1, therefore it changes every timestep and can be used to directly compare to the pre-equilibrium yield. Thus, the final expression for the thermal dilepton yield is given by

$$\frac{dN}{dM^2 d\eta} = \pi R_T^2 \sum_i \tau_i \Delta\tau \frac{\alpha_{EM}^2}{3\pi^3} e^{2\mu/T(\tau_i)} MT(\tau_i) K_1\left(\frac{M}{T(\tau_i)}\right). \quad (5.8)$$

5.3 COMPARISON BETWEEN THERMAL AND PRE-EQUILIBRIUM YIELDS

Figure 14 shows the comparison between the thermal and pre-equilibrium dilepton yield. The pre-equilibrium evolution starts at the time $1/Q_s$ and is evolved until $25/Q_s$. This duration is equivalent to $\sim 0.2 - 5$ fm/c for $Q_s = 1$ GeV and $\sim 0.1 - 2.5$ fm/c for $Q_s = 2$ GeV.

As shown, the thermal yield is greater than the pre-equilibrium yield by approximately two orders of magnitude for the $Q_s = 1$ GeV case and between two to seven orders of magnitude larger when $Q_s = 2$ GeV. As before, this is due to more quark/anti-quark

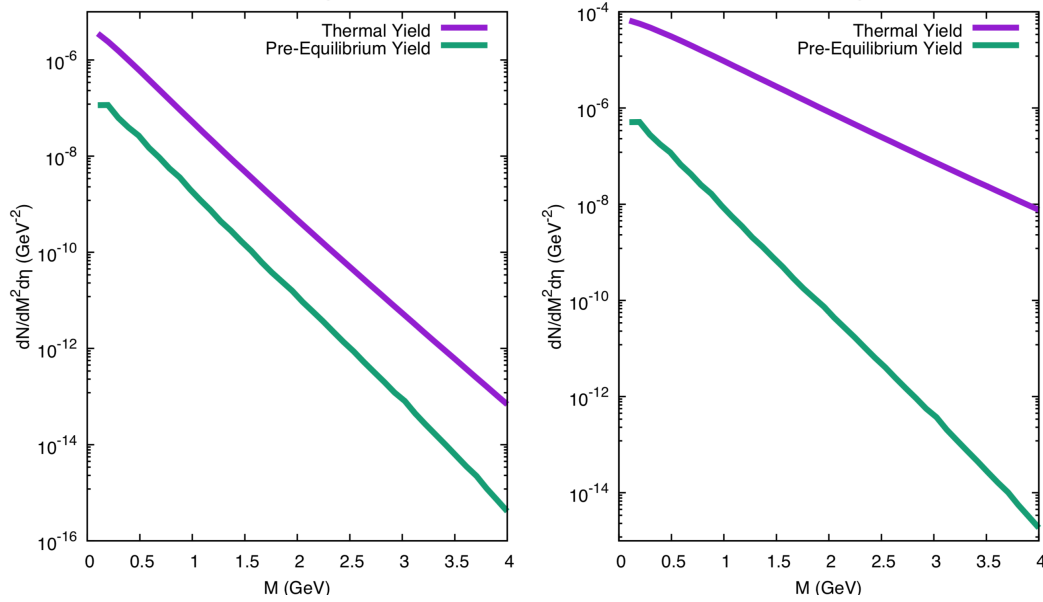


Figure 14: The dilepton yield for the thermal and pre-equilibrium cases are plotted for $Q_s = 1$ GeV (left) and $Q_s = 2$ GeV (right).

pairs present at the time of thermalization in comparison to the pre-equilibrium case. The large difference between the thermal yield for the $Q_s = 1$ GeV and $Q_s = 2$ GeV cases is a result of equation 5.8 being heavily temperature dependent. Thus, when the temperatures are doubled as in the $Q_s = 2$ GeV case, the yield is significantly affected.

PHOTON PRODUCTION IN THERMAL EQUILIBRIUM AND PRE-EQUILIBRIUM QGP

In addition to dileptons, another useful probe of early-time quark-gluon plasma dynamics are photons. In a system comprised of only quarks and gluons, both dileptons and photons are produced through the annihilation of a quark with an anti-quark. However, there is an additional process which produces photons. This is the Compton scattering process shown in figure 5 in which a quark or anti-quark scatters with a gluon. As with dileptons, photons are also very useful as they too only interact electromagnetically with the medium.

This chapter starts by deriving the pre-equilibrium photon production rate in terms of $E dR/d^3p$. The photon production rate in thermal equilibrium is also derived and compared to the pre-equilibrium case.

6.1 PHOTON PRODUCTION RATE IN PRE-EQUILIBRIUM QGP

The rate of production of particles created through collisions of other particles can be determined from kinetic theory using the collision term, which is the right-hand side of the Boltzmann equation. In the case of photons, this production rate can be derived starting with the expression for the production of on-shell photons,

$$E \frac{d^3R}{d^3p} = \int \frac{d^3p_1}{(2\pi)^3 2E_1} \frac{d^3p_2}{(2\pi)^3 2E_2} \frac{d^3p_3}{(2\pi)^3 2E_3} \frac{1}{2(2\pi)^3} |\mathcal{M}_i|^2 (2\pi)^4 \times \delta^4(P_1 + P_2 - P_3 - P) f_1(\mathbf{p}_1) f_2(\mathbf{p}_2) [1 \pm f_3(\mathbf{p}_3)], \quad (6.1)$$

where the degeneracy factor \mathcal{N} is absorbed into the amplitude $|\mathcal{M}_i|^2$. Following the procedure outlined in [24], the expression for the pre-equilibrium photon production rate can be derived using the small-angle approximation which assumes low momentum

transfer between scattering particles. Only the pair annihilation process is considered first, where the amplitude is given by

$$|\mathcal{M}| = \frac{160}{9} 16\pi^2 \alpha \alpha_s \left(\frac{u^2 + t^2}{ut} \right) \quad (6.2)$$

As the t -channel and u -channel contribute equally, only the t -channel is considered and a factor of two is added to account for the missing u -channel. Inserting the amplitude into the expression gives

$$E \frac{d^3 R}{d^3 p} = \frac{1}{2(2\pi)^3} \frac{320}{9} 16\pi^2 \alpha \alpha_s \int_{p_1, p_2, p_3} \frac{u}{t} (2\pi)^4 \delta^4(P_1 + P_2 - P_3 - P) f_q(\mathbf{p}_1) f_q(\mathbf{p}_2) [1 + f_g(\mathbf{p}_3)] \quad (6.3)$$

where

$$\int_p = \int \frac{d^3 p}{(2\pi)^3 2E_p}. \quad (6.4)$$

Expanding kinematic variables in terms of exchanged momentum $\mathbf{q} = \mathbf{p} - \mathbf{p}_1$ yields the equations

$$p = \sqrt{(\mathbf{p}_1 + \mathbf{q})^2} = p_1 + \mathbf{q} \cdot \mathbf{v}_1 + \mathcal{O}(q^2) \quad (6.5)$$

$$p_3 = \sqrt{(\mathbf{p}_2 + \mathbf{q})^2} = p_2 - \mathbf{q} \cdot \mathbf{v}_2 + \mathcal{O}(q^2), \quad (6.6)$$

where $\mathbf{v}_{1,2} = \mathbf{p}_{1,2}/p_{1,2}$. These expressions can be used to rewrite the Mandelstam variables and the sum of the momenta as

$$s = (P_1 + P_2)^2 = 2p_1 p_2 (1 - \mathbf{v}_1 \cdot \mathbf{v}_2) \quad (6.7)$$

$$t = -Q^2 = -q^2 + (\mathbf{q} \cdot \mathbf{v}_1)^2 + \mathcal{O}(q^3) \quad (6.8)$$

$$u = -s - t = -s + \mathcal{O}(q^3) \quad (6.9)$$

$$p_1 + p_2 - p_3 - p = \mathbf{q} \cdot (\mathbf{v}_2 - \mathbf{v}_1) + \mathcal{O}(q^2). \quad (6.10)$$

The delta function is then divided into its energy and momentum components as $\delta(P_1^0 + P_2^0 - P_3^0 - P^0) \delta^3(\mathbf{p}_1 + \mathbf{p}_2 - \mathbf{p}_3 - \mathbf{p})$ which allows the expression to be integrated over \mathbf{p}_3

$$E \frac{d^3 R}{d^3 p} = \frac{1}{2(2\pi)^3} \frac{320}{9} 16\pi^2 \alpha \alpha_s \int \frac{d^3 p_1}{(2\pi)^3 2p_1^0} \frac{d^3 p_2}{(2\pi)^3 2p_2^0} \frac{2\pi}{2(p_2^0 - \mathbf{q} \cdot \mathbf{v})} \frac{u}{t} \times \delta(P_1^0 + P_2^0 - P_3^0 - P^0) f_q(\mathbf{p}_1) f_q(\mathbf{p}_2) [1 + f_g(\mathbf{p}_3)], \quad (6.11)$$

where $p_3^0 = p_2^0 - \mathbf{q} \cdot \mathbf{v}$. Now, after rewriting the remaining energy delta function in terms of the new kinematic variables defined above

$$\delta(p_1^0 + p_2^0 - p_3^0 - p^0) = \delta(p_1^0 + p_2^0 - (p_2^0 - \mathbf{q} \cdot \mathbf{v}_2) - (p_1^0 + \mathbf{q} \cdot \mathbf{v}_1)) \quad (6.12)$$

$$= \delta(\mathbf{q} \cdot (\mathbf{v}_1 - \mathbf{v}_2)), \quad (6.13)$$

the expression becomes

$$E \frac{d^3 R}{d^3 p} = \frac{1}{2(2\pi)^3} \frac{320}{9} 16\pi^2 \alpha \alpha_s \int \frac{d^3 p_1}{(2\pi)^3} \frac{d^3 p_2}{(2\pi)^3} \frac{2\pi}{4(p_2^0 - \mathbf{q} \cdot \mathbf{v})} \frac{(1 - \mathbf{v}_1 \cdot \mathbf{v}_2)}{-q^2 + (\mathbf{q} \cdot \mathbf{v}_1)^2} \times \delta(\mathbf{q} \cdot (\mathbf{v}_1 - \mathbf{v}_2)) f_q(\mathbf{p}_1) f_q(\mathbf{p}_2) [1 + f_g(\mathbf{p}_3)] \quad (6.14)$$

where the new expression for the Mandelstam variables u and t have also been inserted. Using $\mathbf{q} = \mathbf{p} - \mathbf{p}_1$ to rewrite the \mathbf{p}_1 integration as an integration over \mathbf{q} , the expression becomes

$$E \frac{d^3 R}{d^3 p} = \frac{20}{9\pi^3} \alpha \alpha_s \int d^3 q \int \frac{d^3 p_2}{(2\pi)^3} \frac{1}{p_2} \frac{1 - \mathbf{v} \cdot \mathbf{v}_2}{q^2 - (\mathbf{q} \cdot \mathbf{v})^2} \delta(\mathbf{q} \cdot (\mathbf{v}_2 - \mathbf{v})) \times f_q(\mathbf{p}_1) f_q(\mathbf{p}_2) [1 + f_g(\mathbf{p}_3)] \quad (6.15)$$

as $\mathbf{v} \sim \mathbf{v}_1 + \mathcal{O}(q)$. The \mathbf{q} integration is independent of \mathbf{v} and \mathbf{v}_2 , it can be expressed as

$$2\pi \mathcal{L} \equiv \int d^3 q \frac{1 - \mathbf{v}_1 \cdot \mathbf{v}_2}{q^2 - (\mathbf{q} \cdot \mathbf{v}_1)^2} \delta(\mathbf{q} \cdot (\mathbf{v}_2 - \mathbf{v})) = 2\pi \int \frac{dq}{q} \quad (6.16)$$

where the logarithmic divergence is given by

$$\mathcal{L} = \int_{\Lambda_{IR}}^{\Lambda_{UV}} \frac{dq}{q} = \log \frac{\Lambda_{UV}}{\Lambda_{IR}}. \quad (6.17)$$

The IR cutoff is given by the the Debye mass scale $m_D \sim g^2 T^2$ and the UV cutoff is given by the temperature T , which come from thermal field theory. This simplifies the expression such that the production rate from the annihilation process is given by

$$E \frac{d^3 R}{d^3 p} = \frac{40}{9\pi^2} \alpha \alpha_s \mathcal{L} f_q(\mathbf{p}) \int \frac{d^3 p'}{(2\pi)^3} \frac{1}{p'} f_q(\mathbf{p}') [1 + f_g(\mathbf{p}')]. \quad (6.18)$$

For Compton scattering contribution, a similar derivation can be performed which yields the expression

$$E \frac{d^3 R}{d^3 p} = \frac{40}{9\pi^2} \alpha \alpha_s \mathcal{L} f_q(\mathbf{p}) \int \frac{d^3 p'}{(2\pi)^3} \frac{1}{p'} f_g(\mathbf{p}') [1 + f_q(\mathbf{p}')], \quad (6.19)$$

where the s-channel contribution is neglected in this approximation. Summing the Compton and annihilation contributions gives the expression

$$E \frac{d^3 R}{d^3 p} = \frac{40}{9\pi^2} \alpha \alpha_s \mathcal{L} f_q(\mathbf{p}) \int \frac{d^3 p'}{(2\pi)^3} \frac{1}{p'} [f_g(\mathbf{p}') + f_q(\mathbf{p}')]. \quad (6.20)$$

Knowing that $\mathbf{p} = (p_\perp, p_z)$ and $d^3 p = p_\perp dp_\perp dp_z d\phi$, an integral over ϕ can be performed, and the final expression for the pre-equilibrium photon production rate is given by

$$E \frac{d^3 R}{d^3 p} = \frac{40}{9\pi^2} \alpha \alpha_s \mathcal{L} f_q(p_\perp, p_z) \int \frac{p'_\perp dp'_\perp dp'_z}{(2\pi)^2} \frac{1}{\sqrt{p'^2_\perp + p'^2_z}} [f_g(p'_\perp, p'_z) + f_q(p'_\perp, p'_z)] \quad (6.21)$$

where the value of \mathcal{L} is determined at the end of the next section.

6.2 PHOTON PRODUCTION RATE IN THERMAL QGP

As in the pre-equilibrium case, the derivation of the thermal photon production rate starts with the general expression for production rate from kinetic theory given by

$$E \frac{d^3 R}{d^3 p} = \int \frac{d^3 p_1}{(2\pi)^3 2E_1} \frac{d^3 p_2}{(2\pi)^3 2E_2} \frac{d^3 p_3}{(2\pi)^3 2E_3} \frac{1}{2(2\pi)^3} |M_i|^2 (2\pi)^4 \times \delta^4(P_1 + P_2 - P_3 - P) f_1(\mathbf{p}_1) f_2(\mathbf{p}_2) [1 \pm f_3(\mathbf{p}_3)] \quad (6.22)$$

This equation can be rewritten in terms of the Mandelstam variables by inserting the delta functions $s = (p_1 + p_2)^2$ and $t = (p_1 - p_3)^2$

$$E \frac{d^3 R}{d^3 p} = \int ds dt \frac{d^3 p_1 d^3 p_2 d^3 p_3}{16(2\pi)^8 E_1 E_2 E_3} |M_i|^2 e^{-E/T} \delta^4(p_1 + p_2 - p_3 - p) \times \delta(s - (p_1 + p_2)^2) \delta(t - (p_1 - p_3)^2) \quad (6.23)$$

where Maxwell-Boltzmann statistics have been used for the particle distribution functions. Recall the identity $d^3 p_3 \rightarrow d^4 p_3 \theta(E_3) \delta(p_3^2 - m_3^2) 2E_3$, which allows the expression to be written as

$$E \frac{d^3 R}{d^3 p} = \int ds dt \frac{d^3 p_1 d^3 p_2}{8(2\pi)^8 E_1 E_2} |M_i|^2 d^4 p_3 e^{-E/T} \delta(p_3^2 - m_3^2) \theta(E_3) \delta^4(p_1 + p_2 - p_3 - p) \times \delta(s - (p_1 + p_2)^2) \delta(t - (p_1 - p_3)^2) \quad (6.24)$$

The delta function $\delta(p_3^2 - m_3^2)$ can be rewritten by integrating over $d^4 p_3$ using $p_3 = (E_1 + E_2 - E) - (\mathbf{p}_1 + \mathbf{p}_2 - \mathbf{p})$

$$E \frac{d^3 R}{d^3 p} = \int ds dt \frac{d^3 p_1 d^3 p_2}{8(2\pi)^8 E_1 E_2} |M_i|^2 e^{-E/T} \delta(s - (p_1 + p_2)^2) \delta(t - (p_1 - p_3)^2) \times \delta((E_1 + E_2 - E)^2 - (\mathbf{p}_1 + \mathbf{p}_2)^2 - \mathbf{p}^2 + 2\mathbf{p} \cdot (\mathbf{p}_1 + \mathbf{p}_2) - m_3^2) \quad (6.25)$$

which can be further simplified using $s = (E_1 + E_2)^2 - (\mathbf{p}_1 + \mathbf{p}_2)^2$ and $\mathbf{p}_2 = E_2$

$$E \frac{d^3 R}{d^3 p} = \int ds dt \frac{d^3 p_1 d^3 p_2}{8(2\pi)^8 E_1 E_2} |M_i|^2 e^{-E/T} \delta(s - (p_1 + p_2)^2) \delta(t - (p_1 - p_3)^2) \delta((E_1 + E_2 - E)^2 - (E_1 + E_2)^2 + s - E^2 + 2pp_1 \cos\theta_1 + 2pp_2 \cos\theta_2 - m_3^2) \quad (6.26)$$

The energy delta function can be expanded as

$$\begin{aligned} (E_1 + E_2 - E)^2 - (E_1 + E_2)^2 + s - E^2 + 2pp_1 \cos\theta_1 + 2pp_2 \cos\theta_2 - m_3^2 \\ = s - 2EE_1 - 2EE_2 + 2pp_1 \cos\theta_1 + 2pp_2 \cos\theta_2 - m_3^2, \end{aligned} \quad (6.27)$$

and the t delta function as

$$t - (p_1 - p_3)^2 = t - m_2^2 + 2EE_2 - 2pp_2 \cos\theta_2, \quad (6.28)$$

Rearranging this expression to isolate $\cos\theta_2$

$$\cos\theta_2 = \frac{t - m_2^2 + 2EE_2}{2pp_2} \quad (6.29)$$

gives a Jacobian of $\mathcal{J} = \frac{1}{2Ep_2}$. The s delta function is also expanded as

$$s - (p_1 + p_2)^2 = s - m_1^2 - m_2^2 - 2E_1 E_2 + 2\mathbf{p}_1 \cdot \mathbf{p}_2 \quad (6.30)$$

Substituting these back into the integral

$$\begin{aligned} E \frac{d^3 R}{d^3 p} = \int ds dt \frac{d^3 p_1 d^3 p_2}{8(2\pi)^8 E_1 E_2} |M_i|^2 e^{-E/T} \delta(s - 2EE_1 + 2pp_1 \cos\theta_1 - m_3^2 + t - m_2^2) \\ \times \delta(s - m_1^2 - m_2^2 - 2E_1 E_2 + 2\mathbf{p}_1 \cdot \mathbf{p}_2), \end{aligned} \quad (6.31)$$

where $\mathbf{p}_1 \cdot \mathbf{p}_2 = p_1 p_2 [\cos\theta_1 \cos\theta_2 + \sin\theta_1 \sin\theta_2 \cos(\phi_1 - \phi_2)]$. From the energy delta function,

$$\cos\theta_1 = \frac{2EE_1 + m_2^2 + m_3^2 - s - t}{2pp_1}, \quad (6.32)$$

which gives a Jacobian of $\mathcal{J} = \frac{1}{2Ep_1}$. Now rewrite the integration measure as $d^3 p = p^2 dp d\cos\theta d\phi$

$$\begin{aligned} E \frac{d^3 R}{d^3 p} = \int ds dt \frac{p_1 dp_1 d\phi_1 p_2 dp_2 d\phi_2}{8(2\pi)^8 E_1 E_2} |M_i|^2 e^{-E/T} \frac{1}{4E^2} \times \delta(s - m_1^2 - m_2^2 - 2E_1 E_2 \\ + 2p_1 p_2 [\cos\theta_1 \cos\theta_2 + \sin\theta_1 \sin\theta_2 \cos(\phi_1 - \phi_2)]). \end{aligned} \quad (6.33)$$

Setting $\phi_2 = 0$, the delta function gives

$$\cos\phi_1 = \frac{m_1^2 + m_2^2 + 2E_1E_2 - s - 2p_1p_2\cos\theta_1\cos\theta_2}{2p_1p_2\sin\theta_1\sin\theta_2} = \frac{A}{B} \quad (6.34)$$

which gives a Jacobian of $\mathcal{J} = \frac{1}{2p_1p_2\sin\theta_1\sin\theta_2\sin\phi_1}$. Using the well known trigonometric identity $\sin^2\phi_1 + \cos^2\phi_1 = 1$, the Jacobian can be written in terms of the variables A and B as $\mathcal{J} = \frac{1}{\sqrt{B^2 - A^2}}$ where

$$B^2 = 4(E_1^2 - m_1^2)(E_2^2 - m_2^2)(1 - \cos^2\theta_1)(1 - \cos^2\theta_2) \quad (6.35)$$

and

$$A = m_1^2 + m_2^2 + 2E_1E_2 - s - \frac{(2EE_1 + m_2^2 + m_3^2 - s - t)(t - m_2^2 + 2EE_2)}{2E^2}. \quad (6.36)$$

To simplify these expressions, new variables are defined as

$$\beta = s - m_1^2 - m_2^2 \quad (6.37)$$

$$\alpha = m_2^2 - t \quad (6.38)$$

$$\gamma = s + t - m_2^2 - m_3^2. \quad (6.39)$$

such that A and B^2 become

$$A = 2E_1E_2 - \beta - \frac{(2EE_1 - \gamma)(2EE_2 - \alpha)}{2E^2} \quad (6.40)$$

$$B^2 = 4(E_1^2 - m_1^2)(E_2^2 - m_2^2) \left(1 - \frac{(2EE_1 - \gamma)^2}{4E^2(E_1^2 - m_1^2)}\right) \left(1 - \frac{(2EE_2 - \alpha)^2}{4E^2(E_2^2 - m_2^2)}\right) \quad (6.41)$$

After some algebraic manipulation, it can be shown that $\sqrt{B^2 - A^2} = \sqrt{a'E_2^2 + b'E_2 + c'}$, where

$$a' = \frac{-\gamma^2}{E^2} \quad (6.42)$$

$$b' = \frac{2\beta E\gamma + 2\alpha E_1\gamma - 4\alpha E m_1^2}{E^2} \quad (6.43)$$

$$c' = \frac{-\beta^2 E^2 + 2\alpha\beta E E_1 - \alpha^2 E_1^2 - \alpha\beta\gamma + \alpha^2 m_1^2 - 4E E_1\gamma m_2^2 + \gamma^2 m_2^2 + 4E^2 m_1^2 m_2^2}{E^2} \quad (6.44)$$

Finally, the Jacobian can be written as

$$\frac{1}{\sqrt{B^2 - A^2}} = \frac{E}{\sqrt{a'E_2^2 + b'E_2 + c}} \quad (6.45)$$

where

$$a = -(s + t - m_2^2 - m_3^2)^2 \quad (6.46)$$

$$b = 2(s - m_1^2 - m_2^2)(s + t - m_2^2 - m_3^2)E + 2(m_2^2 - t)(s + t - m_2^2 - m_3^2)E_1 - 4(m_2^2 - t)Em_1^2 \quad (6.47)$$

$$c = c_2E_1^2 + c_1E_1 + c_0 \quad (6.48)$$

$$(6.49)$$

and

$$c_2 = -(m_2^2 - t)^2 \quad (6.50)$$

$$c_1 = 2(m_2^2 - t)(s - m_1^2 - m_2^2)E - 4(s + t - m_2^2 - m_3^2)m_2^2E \quad (6.51)$$

$$c_0 = -(s - m_1^2 - m_2^2)^2E^2 - (m_2^2 - t)(s - m_1^2 - m_2^2)(s + t - m_2^2 - m_3^2) + (m_2^2 - t)^2m_1^2 + (s + t - m_2^2 - m_3^2)^2m_2^2 + 4E^2m_1^2m_2^2. \quad (6.52)$$

Returning to the integral using $p_1dp_1 \rightarrow E_1dE_1$, $p_2dp_2 \rightarrow E_2dE_2$ and integrating over ϕ_1

$$E \frac{d^3R}{d^3p} = \frac{N}{(2\pi)^7} \frac{1}{16E} \int ds dt dE_1 dE_2 |M_i|^2 e^{-E/T} \frac{1}{\sqrt{aE_2^2 + bE_2 + c}}. \quad (6.53)$$

where the additional factor of 2 comes from the fact that $\cos\phi_1$ will be satisfied twice with ϕ_0 and $-\phi_0$ when integrating from $\phi = 0$ to $\phi = 2\pi$.

Now the limits of integration are to be calculated. For E_2 , the limits come from the fact that the argument inside the square root must be greater than zero. Therefore, this gives the limits

$$\frac{-b - \sqrt{b^2 - 4ac}}{2a} \leq E_2 \leq \frac{-b + \sqrt{b^2 - 4ac}}{2a} \quad (6.54)$$

where $E_1 + E_2 - E \geq 0$. As s has no restrictions from the equation, the lower limit is chosen such that it cannot be lower than the sum of the masses of the incoming particle or lower than the mass of the outgoing particle. Therefore, $s_{min} = (m_1 + m_2)^2, m_3^2$ and $s_{max} = \infty$ as there is no strict upper limit.

Using the $\cos\theta_1$ expression determined earlier, the limits of E_1 can be determined such that

$$\cos\theta_1 = \left| \frac{2EE_1 + m_2^2 + m_3^2 - s - t}{2pp_1} \right| = \pm 1. \quad (6.55)$$

which gives

$$t = 2EE_1 + m_2^2 + m_3^2 - s \pm 2Ep_1. \quad (6.56)$$

From the expression $\sqrt{s} = \sqrt{m_1^2 + \mathbf{p}_1^2} + \sqrt{m_2^2 + \mathbf{p}_1^2}$, E_1 can be written as

$$E_1 = \frac{s + m_1^2 - m_2^2}{2\sqrt{s}} \quad (6.57)$$

and p_1 can be rewritten from $p_1^2 + m_1^2 = \frac{(s + m_1^2 - m_2^2)^2}{4s}$ as

$$p_1 = \frac{\lambda^{1/2}(s, m_1^2, m_2^2)}{2\sqrt{s}}. \quad (6.58)$$

after some algebraic manipulation. Inserting these expressions for E_1 and p_1 back into expression for t gives

$$t_{\pm} = m_2^2 + m_3^2 - s + E \left(\frac{s + m_1^2 - m_2^2}{\sqrt{s}} \right) \pm E \left(\frac{\lambda^{1/2}(s, m_1^2, m_2^2)}{\sqrt{s}} \right). \quad (6.59)$$

However, knowing that $t = (p_1 - p_3)^2$, this can be expanded as

$$t = m_2^2 - 2EE_2 + 2\mathbf{p} \cdot \mathbf{p}_2. \quad (6.60)$$

Also knowing that $\sqrt{s} = E + \sqrt{m_3^2 + \mathbf{p}_3^2}$, E can be rewritten as

$$E = \frac{s - m_3^2}{2\sqrt{s}}. \quad (6.61)$$

Inserting these into the t_{\pm} expression, the limits for t are obtained

$$t_{\pm} = m_2^2 + m_3^2 - s + \frac{(s - m_3^2)(s + m_1^2 - m_2^2)}{2s} \pm \frac{(s - m_3^2)\lambda^{1/2}(s, m_1^2, m_2^2)}{2s}. \quad (6.62)$$

where t_+ represents the upper limit and t_- denotes the lower limit.

The limits for E_1 can be determined from the $\cos\theta_1$ such that $2Ep_1\cos\theta_1 = m_2^2 + m_3^2 - t - s + 2EE_1$. This gives a lower limit on E_1 of

$$E_1 \geq \frac{s + t - m_2^2 - m_3^2}{4E} + \frac{Em_1^2}{s + t - m_2^2 - m_3^2} \quad (6.63)$$

and the upper limit is taken to infinity. Similarly, the limits for E_2 come from the $\cos\theta_2$ expression such that $t - m_2^2 + 2EE_2 = 2Ep_2\cos\theta_2$. This gives a lower limit for E_2 of

$$E_2 \geq \frac{m_2^2 - t}{4E} + \frac{E^2 m_2^2}{m_2^2 - t}. \quad (6.64)$$

and the upper limit is again taken to infinity. Also note that the equalities $m_2^2 - t \geq 0$ and $E_1 + E_2 - E \geq 0$ must be satisfied so as to ensure energy conservation.

After accounting for infrared contributions, an analytical solution for the thermal photon production rate, taken from [20], is given by

$$E \frac{dR}{d^3p} = \frac{5}{9} \frac{\alpha_{EM} \alpha_s}{2\pi^2} T^2 e^{-E/T} \ln\left(\frac{2.912 E}{g^2 T} + 1\right) \quad (6.65)$$

which assumes that $E \gg T$. Figure 15 shows how this solution compares to the numerical integration of equation 6.53 using a temperature of 0.2 GeV. For energies greater than 0.4 GeV, the analytical solution matches the results of the numerical integration.

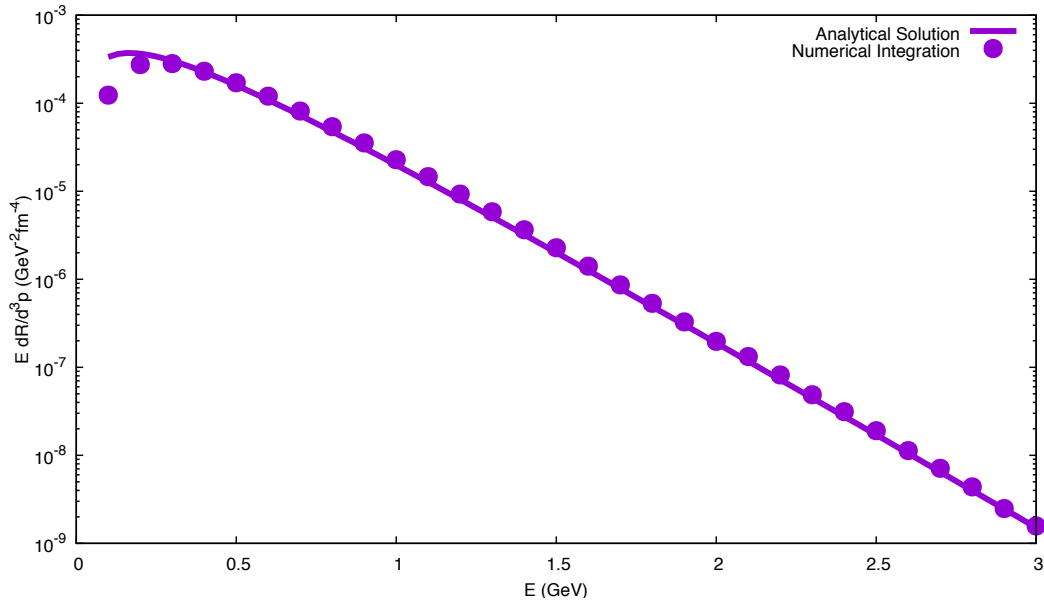


Figure 15: The analytical solution of the thermal photon rate is plotted and compared to the numerical integration of equation 6.53 using $T = 200$ MeV.

The analytical solution to the thermal photon rate was then used to compare to that determined from small-angle approximation, taken from [24], which is given by

$$E \frac{d^3R}{d^3p} = \frac{10}{9} \frac{\alpha_{EM} \alpha_s}{2\pi^2} T^2 \mathcal{L} e^{-E/T}. \quad (6.66)$$

which again assumes that $E \gg T$, where the value of \mathcal{L} still needs to be determined. However, \mathcal{L} contains cutoff scales which cannot be determined from first principles. Therefore, this derivation was done by adjusting the value of \mathcal{L} until a good match between the analytical solution given by 6.65 and 6.66 was achieved. A value of $\mathcal{L} = 0.75$ was chosen and the comparison is shown in figure 16.

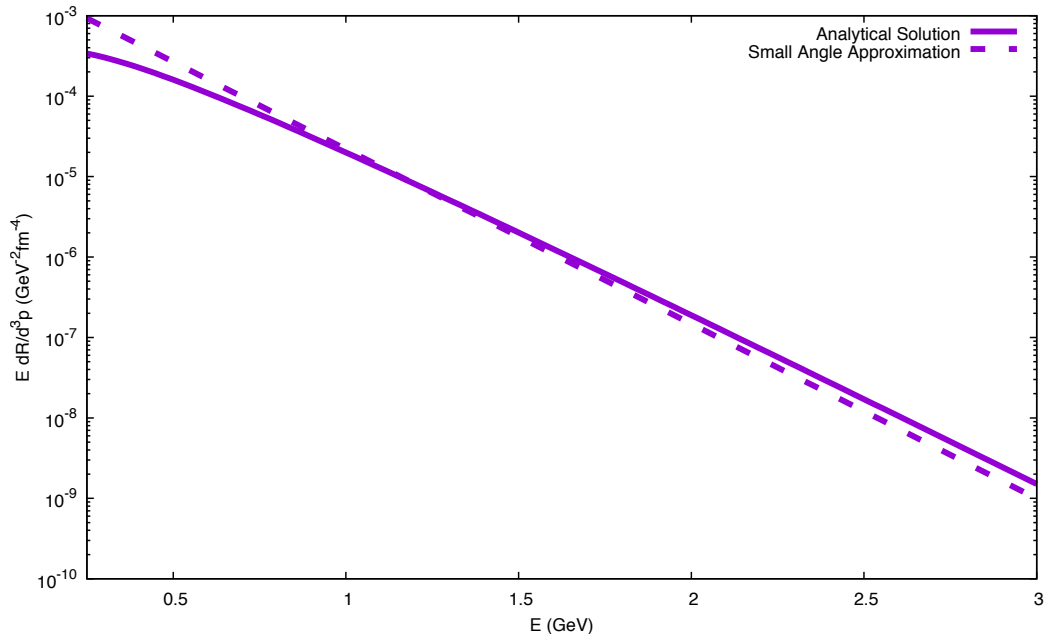


Figure 16: The analytical solution of the thermal photon rate given by 6.65 is plotted and compared to the rate determined using the small-angle approximation given by 6.66 for $T = 200$ MeV. A value of $\mathcal{L} = 0.75$ was chosen to best match the two results.

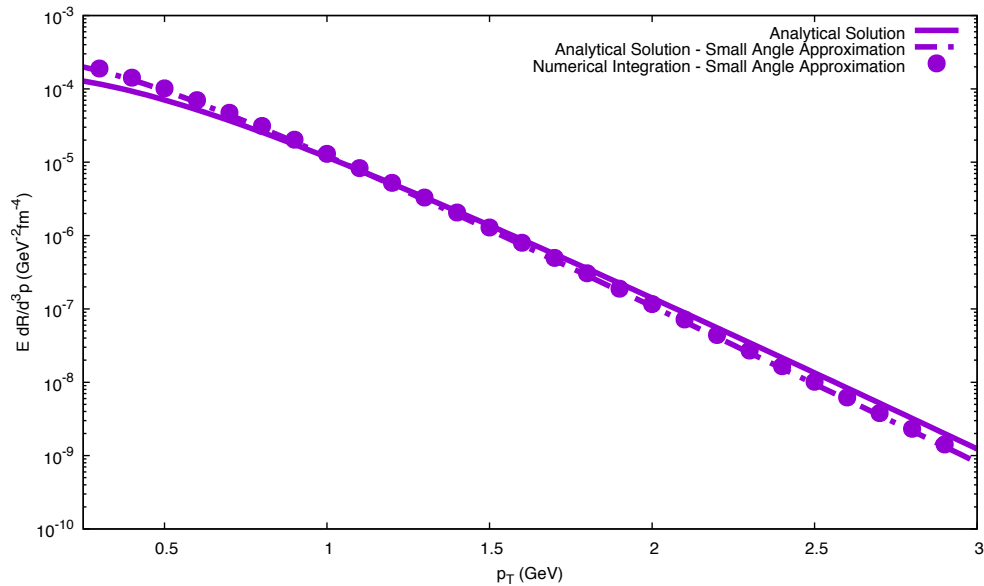


Figure 17: The analytical solution of the thermal photon rate (eq. 6.65) is plotted and compared to the analytical solution (eq. 6.66) and the numerical integration of the rate (eq. 6.67) determined using small-angle approximation for a fixed $p_z = 0.5$ GeV.

The thermal photon production rate can also be plotted as a function of transverse momentum, where $E = \sqrt{p_{\perp}^2 + p_z^2}$ in equations 6.65 and 6.66, and the equation

$$E \frac{d^3 R}{d^3 p} = \frac{40}{9\pi^2} \alpha \alpha_s \mathcal{L} e^{\sqrt{p_{\perp}^2 + p_z^2}/T} \int \frac{p'_{\perp} dp'_{\perp} dp'_z}{(2\pi)^2} \frac{1}{\sqrt{p'^2_{\perp} + p'^2_z}} e^{\sqrt{p'^2_{\perp} + p'^2_z}/T} \quad (6.67)$$

can be numerically integrated to test the accuracy of the computation. This comparison is shown in figure 17, where it is clear that both the analytical solution as well as the numerical integration of the thermal photon rate calculated from the small-angle approximation are comparable to the analytical solution calculated without the approximation.

6.3 COMPARISON BETWEEN THERMAL AND PRE-EQUILIBRIUM PRODUCTION RATES

In the previous section, it was shown that the small-angle approximation yields a reasonable solution to the thermal photon production rate. Therefore, this solution is also used for the pre-equilibrium photon production rate. As in the dilepton case, the photon production rates were derived assuming only massless up and down quarks, so a factor of 6/5 is again used to modify these rates for account for the additional quark included in the procedure for solving the Boltzmann equation. The chemical potential was also added to the thermal rate to ensure consistency with the pre-equilibrium case. The modified expression for the pre-equilibrium rate is

$$E \frac{d^3 R}{d^3 p} = \frac{16}{3\pi^2} \alpha \alpha_s \mathcal{L} f_q(p_{\perp}, p_z) \int \frac{p'_{\perp} dp'_{\perp} dp'_z}{(2\pi)^2} \frac{1}{\sqrt{p'^2_{\perp} + p'^2_z}} [f_g(p'_{\perp}, p'_z) + f_q(p'_{\perp}, p'_z)] \quad (6.68)$$

and

$$E \frac{d^3 R}{d^3 p} = \frac{4}{3} \frac{\alpha_{EM} \alpha_s}{2\pi^2} T^2 \mathcal{L} e^{-(E-2\mu)/T} \quad (6.69)$$

$$E \frac{dR}{d^3 p} = \frac{2}{3} \frac{\alpha_{EM} \alpha_s}{2\pi^2} T^2 e^{-(E-2\mu)/T} \ln \left(\frac{2.912 E}{g^2 T} + 1 \right) \quad (6.70)$$

are the modified expressions for the thermal photon production rate with and without the small-angle approximation.

The pre-equilibrium evolution starts with an initial time $1/Q_s$ and is evolved until $25/Q_s$. The expression given by 6.68 was numerically integrated using the distribution functions calculated by [19]. As before, in the case of dileptons, the timestep $2/Q_s$ was chosen for the pre-equilibrium case which corresponds to $T = 218$ MeV, $\mu = -0.29$ GeV for $Q_s = 1$ GeV and $T = 436$ MeV, $\mu = -0.58$ GeV for $Q_s = 2$ GeV which were calculated by solving the system of equations described in section 4.3.1. As expected from the dilepton results, the pre-equilibrium photon production rate is lower than the thermal equilibrium rate by about one to two orders of magnitude. This is again due to the lack of quarks/anti-quarks present in the pre-equilibrium case, as shown in figure 10.

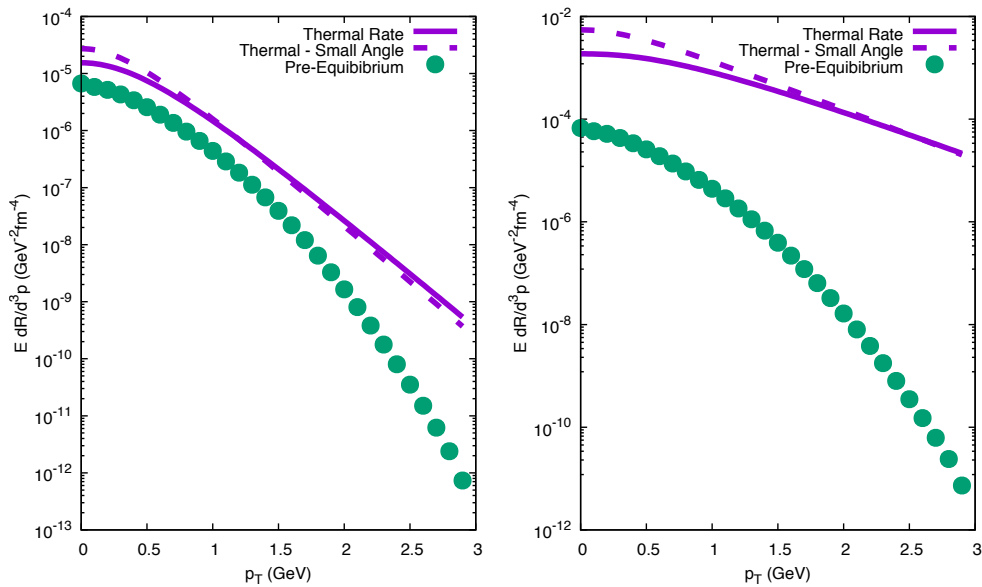


Figure 18: The analytical solution of the thermal photon rate for a fixed $p_z = 0.5$ GeV (eq. 6.65) is plotted and compared to the analytical solution (eq. 6.66) and the numerical integration of the pre-equilibrium rate determined using small-angle approximation (eq. 6.21) for $Q_s = 1$ GeV, $T = 160$ MeV (left) and $Q_s = 2$ GeV, $T = 320$ MeV (right).

The thermal photon production rate can also be plotted as a function of proper time τ where each timestep for the pre-equilibrium case corresponds to a different temperature in the thermal case. The results of this comparison are shown in figure 19. This figure shows low production rate at very early times due to the lack of quark/anti-quark pairs present in the medium. Once a sufficient number of quarks/anti-quarks have been produced, the pre-equilibrium photon production rate remains about one order of mag-

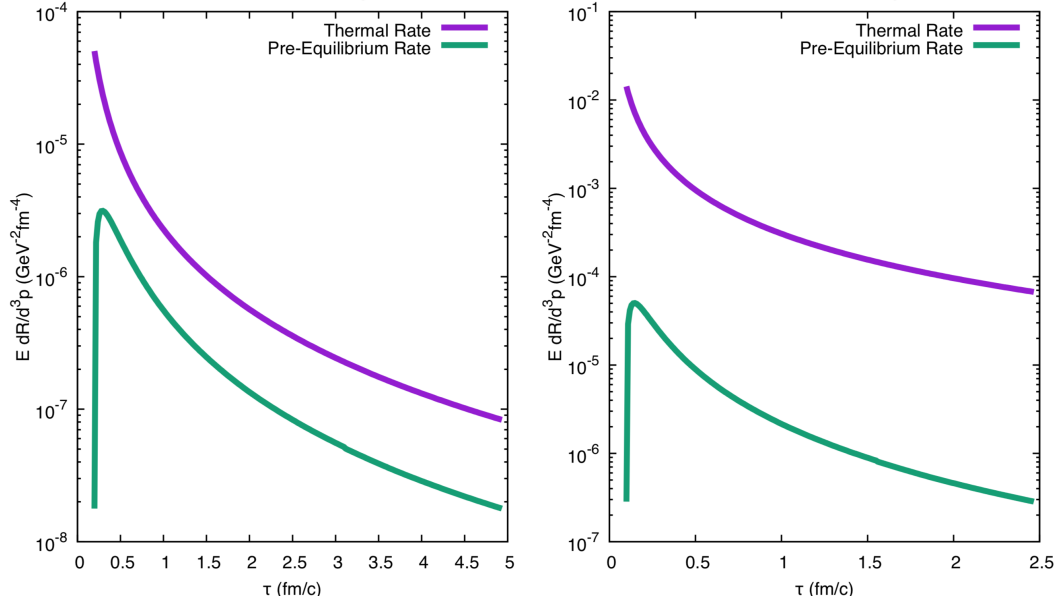


Figure 19: The photon production rate in thermal equilibrium is plotted and compared to the pre-equilibrium rate as a function of time for $Q_s = 1 \text{ GeV}$ (left) and $Q_s = 2 \text{ GeV}$ (right) with fixed $p_z, p_T = 0.5 \text{ GeV}$.

nitude lower for $Q_s = 1 \text{ GeV}$ and about two to three orders of magnitude lower for $Q_s = 2 \text{ GeV}$ throughout the evolution of the medium.

PHOTON YIELD IN THERMAL EQUILIBRIUM AND PRE-EQUILIBRIUM QGP

Studying the rate at which particles are produced after a heavy ion collision has occurred is useful for investigating the evolution of the system. Experimentally, only the yield of produced particles is measurable, and the rate of production cannot be directly observed. In this section, the photon yield for both thermal equilibrium and pre-equilibrium cases are derived and compared.

7.1 PHOTON YIELD IN PRE-EQUILIBRIUM QGP

In order to calculate the photon yield, the photon production rate must be converted using

$$E \frac{d^3R}{d^3p} = E \frac{dN}{d^4X d^3p} = \frac{dN}{\tau d\tau d^2\mathbf{x}_\perp d\eta dy_p d^2\mathbf{p}_\perp}. \quad (7.1)$$

This means that an integral over η and τ is needed in order to obtain an expression of the form $dN/dy_p d^2\mathbf{p}_\perp$.

Previously, in the photon production rate calculation, it was assumed that $\eta = 0$. Therefore, the η dependence needs to be restored for non-zero values of η . To do this, a change of variables from $p_z(\eta) = \tilde{p}_z = p_\perp \sinh(y_p - \eta)$ is performed. However, this can be further rewritten knowing that $p_z = p_\perp \sinh(y_p)$, so that change of variables becomes

$$\tilde{p}_z = p_\perp \sinh(\sinh^{-1}(p_z/p_\perp) - \eta) \quad (7.2)$$

such that $p_z(0) = p_z$ returns the original equation. Thus, upon performing this change of variables and noting that the distribution functions are also a function of τ , an integration over η and τ gives

$$\begin{aligned} \frac{dN}{d^2\mathbf{x}_\perp dy_p d^2\mathbf{p}_\perp} &= \frac{16}{3\pi^2} \alpha \alpha_s \mathcal{L} \int \tau d\tau d\eta f_q(p_\perp, \tilde{p}_z, \tau) \int \frac{p'_\perp dp'_\perp dp'_z}{(2\pi)^2} \frac{1}{\sqrt{p'^2_\perp + p'^2_z}} \\ &\quad \times [f_g(p'_\perp, p'_z, \tau) + f_q(p'_\perp, p'_z, \tau)], \end{aligned} \quad (7.3)$$

where the p' integral is independent of both η and y_p and does not require a change of variables. As in the dilepton case, the integration over x_\perp is simply the overlapping area of the two colliding nuclei which is given by πR_T^2 for perfectly central collisions where $R_T = 1.2A^{1/3}$ [34] is the radius of the nucleus in the transverse plane. The expression for the pre-equilibrium photon yield can therefore be written as

$$\begin{aligned} \frac{dN}{dy_p d^2\mathbf{p}_\perp} &= \frac{16R_T^2}{3\pi} \alpha \alpha_s \mathcal{L} \int \tau d\tau d\eta f_q(p_\perp, \tilde{p}_z, \tau) \int \frac{p'_\perp dp'_\perp dp'_z}{(2\pi)^2} \frac{1}{\sqrt{p'^2_\perp + p'^2_z}} \\ &\quad \times [f_g(p'_\perp, p'_z, \tau) + f_q(p'_\perp, p'_z, \tau)]. \end{aligned} \quad (7.4)$$

Finally, this must be converted to a sum over all timesteps from $1/Q_s$ to $25/Q_s$, so the final expression for the pre-equilibrium photon yield is given by

$$\begin{aligned} \frac{dN}{dy_p d^2\mathbf{p}_\perp} &= \frac{16R_T^2}{3\pi} \alpha \alpha_s \mathcal{L} \sum_{i,j} \tau_i \Delta\tau \Delta\eta f_q(p_\perp, \tilde{p}_z, \tau_i) \int \frac{p'_\perp dp'_\perp dp'_z}{(2\pi)^2} \frac{1}{\sqrt{p'^2_\perp + p'^2_z}} \\ &\quad \times [f_g(p'_\perp, p'_z, \tau_i) + f_q(p'_\perp, p'_z, \tau_i)]. \end{aligned} \quad (7.5)$$

7.2 PHOTON YIELD IN THERMAL QGP

As in the previous section, the thermal photon rate can be converted to a yield using

$$E \frac{dN}{d^4X d^3p} = \frac{dN}{\tau d\tau d^2\mathbf{x}_\perp d\eta dy_p d^2\mathbf{p}_\perp}, \quad (7.6)$$

where, once again, an integral over η and τ is needed in order to obtain an expression of the form $dN/dy_p d^2\mathbf{p}_\perp$. As before, the η and τ dependence can be restored to the expression using

$$\tilde{p}_z = p_\perp \sinh(\sinh^{-1}(p_z/p_\perp) - \eta) \quad (7.7)$$

so the thermal photon yield equation becomes

$$\frac{dN}{dy_p d^2\mathbf{p}_\perp} = \frac{16R_T^2}{3\pi} \alpha\alpha_s \mathcal{L} \int \tau d\tau d\eta e^{-(\sqrt{p_\perp^2 + \tilde{p}_z^2} - \mu)/T} \int \frac{p'_\perp dp'_\perp dp'_z}{(2\pi)^2} \frac{e^{-(\sqrt{p'^2_\perp + p'^2_z} - \mu)/T}}{\sqrt{p'^2_\perp + p'^2_z}} \quad (7.8)$$

where the factor of πR_T^2 is from the integration over x_\perp . The τ and η integrals can now be converted to a sum where temperature is a function of τ and therefore changes every timestep. Thus, the final expression for the thermal photon yield is

$$\frac{dN}{dy_p d^2\mathbf{p}_\perp} = \frac{16R_T^2}{3\pi} \alpha\alpha_s \mathcal{L} \sum_{i,j} \tau_i \Delta\tau \Delta\eta e^{-(\sqrt{p_\perp^2 + \tilde{p}_z^2} - \mu)/T} \int \frac{p'_\perp dp'_\perp dp'_z}{(2\pi)^2} \frac{e^{-(\sqrt{p'^2_\perp + p'^2_z} - \mu)/T}}{\sqrt{p'^2_\perp + p'^2_z}}. \quad (7.9)$$

7.3 COMPARISON BETWEEN THERMAL AND PRE-EQUILIBRIUM YIELDS

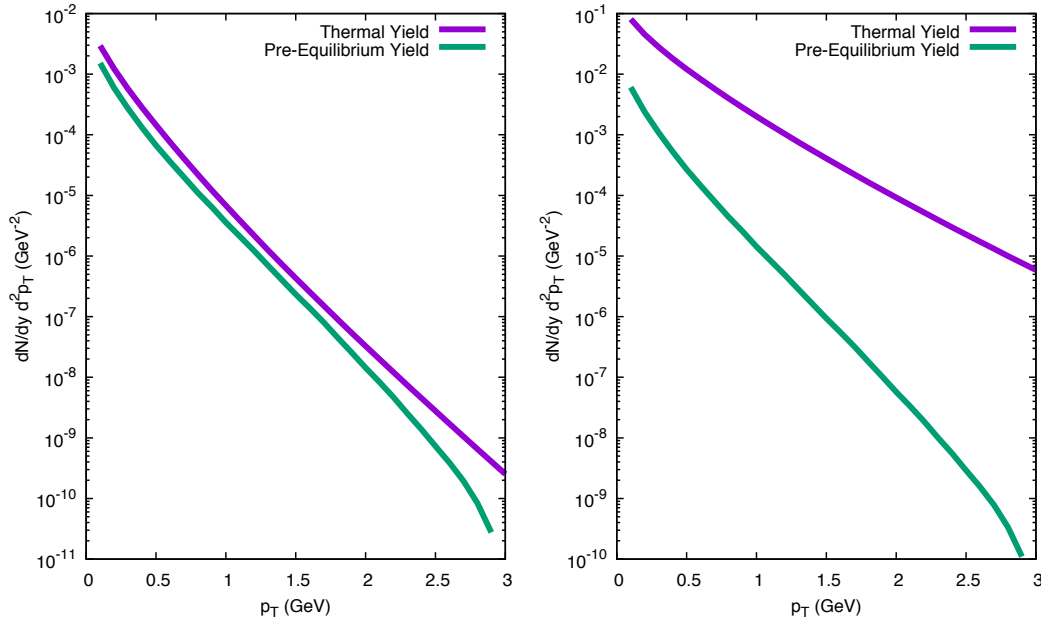


Figure 20: The photon yield for the thermal and pre-equilibrium cases are plotted for $Q_s = 1$ GeV (left) and $Q_s = 2$ GeV (right) for a fixed value of $p_z = 0.5$ GeV.

The thermal and pre-equilibrium photon yields are plotted in figure 20 for $Q_s = 1$ GeV and $Q_s = 2$ GeV. The yields were modified by the factor $6/5$ as before to account for the addition of the strange quark. In the $Q_s = 2$ GeV case, the thermal photon yield is commensurate with other calculations of the thermal yield [17], and the pre-equilibrium results for both Q_s values are lower than the thermal case as expected. As before, this

is due to more quark/anti-quark pairs present in thermal equilibrium in comparison to the pre-equilibrium case.

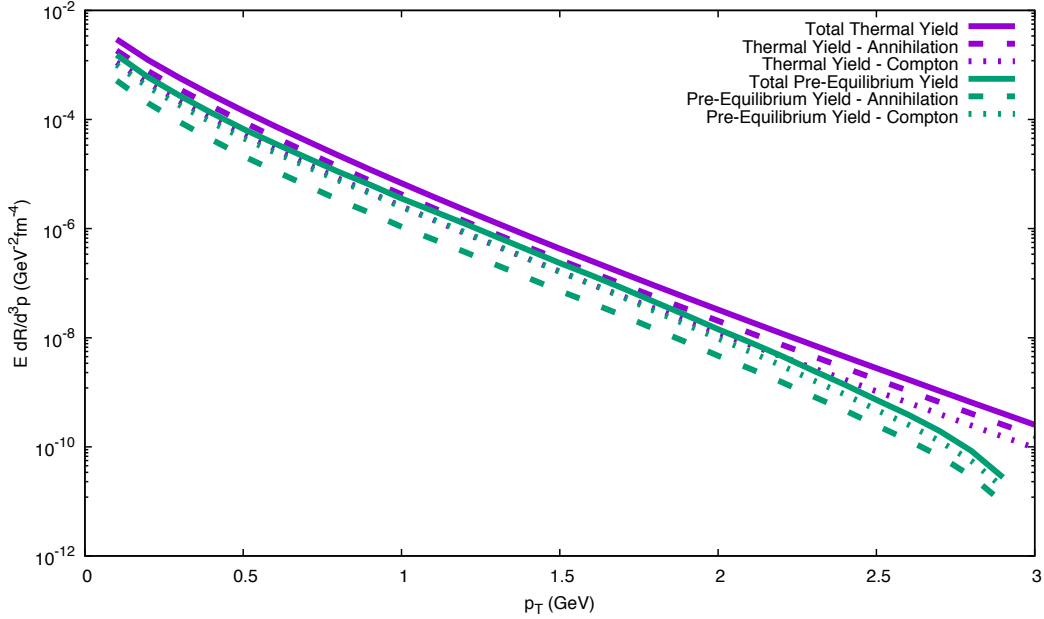


Figure 21: The contribution to the thermal and pre-equilibrium photon yield from the Compton scattering and quark/anti-quark annihilation channels are compared to the total photon yield, the sum of these channels, for $Q_s = 1$ GeV and a fixed value of $p_z = 0.5$ GeV.

Interestingly, for the $Q_s = 1$ GeV case, the pre-equilibrium yield is of the same order of magnitude as the thermal yield, specifically for $p_T \geq 2$ GeV. As the number density of quarks in the thermal medium is consistently larger than the gluon number density (figure 10), the dominant contribution to the thermal photon yield comes from quark/anti-quark annihilation. In contrast, the pre-equilibrium medium has consistently larger gluon number density than the thermal medium, and initially has a very low number density of quarks. Due to the lack of quark/anti-quark pairs, the annihilation channel is much lower than the thermal case, therefore causing the Compton scattering channel to become the dominant contribution to the pre-equilibrium photon yield. This is evident in figure 21 which shows that although the Compton scattering channel in both the pre-equilibrium and thermal cases are approximately equal, the contribution from quark/anti-quark annihilation is much lower in the pre-equilibrium case, causing the total pre-equilibrium photon yield to be consistently lower than the thermal case.

CONCLUSION

When two heavy ions collide, a plasma is created which exists for a very brief period of time. This plasma starts out as a system comprised almost entirely of gluons and evolves as quarks and anti-quarks are created. Eventually, this system reaches a state near thermal equilibrium before the process of hadronization takes place. Probes such as dileptons and photons are used to investigate the underlying physics. These particles make excellent probes as they are created throughout the entirety of the evolution and they interact with the medium only electromagnetically, meaning they can escape the medium without undergoing significant interactions with it and can therefore provide information directly.

In this thesis, the dilepton and photon production rates were calculated for both the pre-equilibrium and thermal equilibrium cases. In addition, the photon and dilepton yields were also computed. The focus of this work was to investigate the nature of the particle production rates and yields in the pre-equilibrium case in comparison to that of the thermal case. The effect of the saturation momentum Q_s was also studied.

In the procedure for calculating the pre-equilibrium distribution functions by solving the Boltzmann equation described in Chapter 3, a non-zero value of the chemical potential μ was assumed and massless up, down, and strange quarks were used. However, in the derivation of the thermal rates and yields, the chemical potential μ was set to zero for simplicity and only massless up and down quarks were used. For the case of non-zero μ , the thermal distribution functions are modified as $e^{-E/T} \rightarrow e^{-(E-2\mu)/T}$, thus yielding an additional factor of $e^{2\mu/T}$. By enforcing that the number and energy density are the same in both the pre-equilibrium and thermal cases, the numerical value of this factor was determined. Additionally, both the thermal and pre-equilibrium rates were modified by a factor of $6/5$ to account for the extra quark.

In almost all cases, the pre-equilibrium results were several orders of magnitude lower than the thermal results. By analyzing a plot of the number density of quarks and gluons, it was shown that the pre-equilibrium quark-gluon plasma initially had a significantly lower number density of quarks and a greater number density of gluons than the thermal case. This explains why the thermal production rates and yields are much larger than the pre-equilibrium cases as there are simply not enough quarks present to interact and produce dileptons and photons. This is in spite of the large energies which characterize the very early times.

The photon yield for $Q_s = 1$ GeV showed interesting results as the pre-equilibrium yield was of the same order of magnitude as the thermal yield for $p_T > 2$ GeV. This was found to be caused by the large number density of gluons and small initial number density of quarks in the pre-equilibrium medium which allowed the Compton scattering contribution of the pre-equilibrium and thermal photon yield to be approximately equal while the annihilation contribution was much less in the pre-equilibrium case. Therefore, after summing the two channels, the total pre-equilibrium yield was only slightly less than the thermal yield.

Additionally, the effect of the Q_s value on the production rates and yields was studied and was shown to have significant effects on the results. Specifically, doubling the value from 1 to 2 GeV had drastically increased these results, especially for the thermal cases. This was due to the implicit temperature and chemical potential dependence of the thermal equations, as both of these quantities doubled with the doubling of Q_s , therefore significantly increasing the rates and yields.

Future work involves extending the model described in Chapter 3 to a more realistic, three-dimensional model. This work can also be used in hydrodynamic calculations to account for the pre-equilibrium electromagnetic radiation. Furthermore, these results are useful for calculations of photon and dilepton elliptic flow v_2 [35].

Part IV

APPENDIX

APPENDIX A

A.1 ENERGY DENSITY - MAXWELL-BOLTZMANN STATISTICS

From relativistic kinetic theory, the energy density is given by

$$\epsilon = v_g \int \frac{d^3 \mathbf{p}}{(2\pi)^3} p^0 f_g(p^0) + v_q \int \frac{d^3 \mathbf{p}}{(2\pi)^3} p^0 f_q(p^0), \quad (\text{A.1})$$

where $v_{g/q}$ and $f_{g/q}$ the degeneracy factors and particle distribution functions for gluons and quarks respectively. Using Maxwell-Boltzmann statistics, the distribution functions are of the form

$$f_{q/g} = e^{-p^0/T} \quad (\text{A.2})$$

where the same distribution function is used for both quarks and gluons. Inserting this into the above equation gives

$$\epsilon = v_g \int \frac{d^3 \mathbf{p}}{(2\pi)^3} p^0 e^{-p^0/T} + v_q \int \frac{d^3 \mathbf{p}}{(2\pi)^3} p^0 e^{-p^0/T}. \quad (\text{A.3})$$

To simplify the integral, a change of variables to $\tilde{p} = p^0/T$ is performed

$$\epsilon = v_g T^4 \int \frac{d^3 \tilde{p}}{(2\pi)^3} \tilde{p} e^{-\tilde{p}} + v_q T^4 \int \frac{d^3 \tilde{p}}{(2\pi)^3} \tilde{p} e^{-\tilde{p}}. \quad (\text{A.4})$$

Recalling that $d^3 \tilde{p} = |\tilde{p}|^2 d\tilde{p} d\Omega$ and that the integral over the solid angle yields a factor of 4π , the expression becomes

$$\epsilon = v_g T^4 (4\pi) \int \frac{|\tilde{p}|^2 d\tilde{p}}{(2\pi)^3} \tilde{p} e^{-\tilde{p}} + v_q T^4 (4\pi) \int \frac{|\tilde{p}|^2 d\tilde{p}}{(2\pi)^3} \tilde{p} e^{-\tilde{p}}. \quad (\text{A.5})$$

After factoring out the degeneracy factors, the remaining integral over \tilde{p} can be computed from

$$\epsilon = (v_g + v_q) \frac{T^4}{2\pi^2} \int_0^\infty |\tilde{p}|^3 e^{-\tilde{p}} d\tilde{p} \quad (\text{A.6})$$

$$= (v_g + v_q) \frac{6T^4}{2\pi^2}. \quad (\text{A.7})$$

If the degeneracy factors are given by

$$\nu_g = 8_{colour} \times 2_{spin} = 16 \quad (\text{A.8})$$

$$\nu_q = 2_{q\bar{q}} \times 2_{spin} \times 3_{flavour} \times 3_{colour} = 36, \quad (\text{A.9})$$

the final expression becomes

$$\epsilon = \frac{156T^4}{\pi^2}. \quad (\text{A.10})$$

If the energy density is well defined as a function of the proper time τ , the equation can be rearranged

$$T = \left(\frac{\epsilon(\tau)}{156/\pi^2} \right)^{1/4} \quad (\text{A.11})$$

to determine the temperature at a given time in the evolution. If the units of the momentum are given in terms of Q_s and the units of the energy density are given as Q_s^4 , therefore, T has units of Q_s . The plot in figure 22 shows the temperature evolution as a function of τ for two values of Q_s .

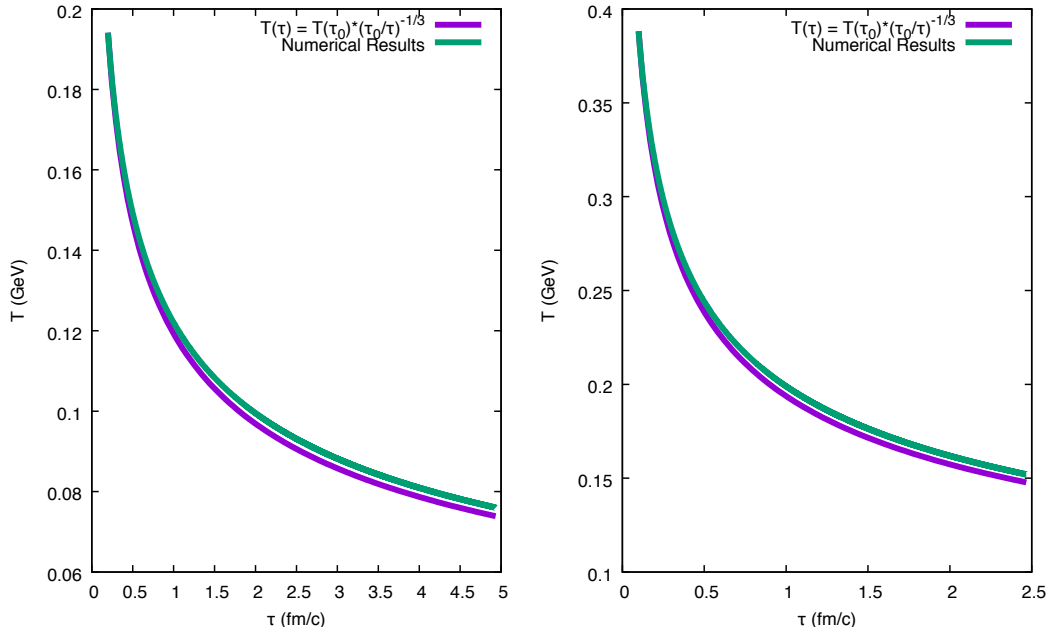


Figure 22: The temperature evolution as a function of τ for $Q_s = 1$ GeV (left) and $Q_s = 2$ GeV (right) is plotted in comparison with the temperature evolution given by the Bjorken solution.

A.2 ENERGY DENSITY - FERMI-DIRAC/BOSE-EINSTEIN STATISTICS

The energy density can also be calculated using Fermi-Dirac and Bose-Einstein statistics, in which case, the distribution functions are of the form

$$f_{q/g} = \frac{1}{e^{p^0/T} \pm 1} \quad (\text{A.12})$$

where the + sign is for quarks (fermions) and the - sign is for gluons (bosons). Inserting these into the energy density equation given by A.1

$$\epsilon = v_g \int \frac{d^3\mathbf{p}}{(2\pi)^3} p^0 \frac{1}{e^{p^0/T} - 1} + v_q \int \frac{d^3\mathbf{p}}{(2\pi)^3} p^0 \frac{1}{e^{p^0/T} + 1}. \quad (\text{A.13})$$

As before, a change of variables to $\tilde{p} = p^0/T$ is performed

$$\epsilon = v_g T^4 \int \frac{d^3\tilde{p}}{(2\pi)^3} \tilde{p} \frac{1}{e^{\tilde{p}} - 1} + v_q T^4 \int \frac{d^3\tilde{p}}{(2\pi)^3} \tilde{p} \frac{1}{e^{\tilde{p}} + 1}. \quad (\text{A.14})$$

Changing the integration measure to $d^3\tilde{p} = |\tilde{p}|^2 d\tilde{p} d\Omega$ and integrating over solid angle gives

$$\epsilon = \frac{v_g T^4}{2\pi^2} \int_0^\infty \frac{|\tilde{p}|^3 d\tilde{p}}{e^{\tilde{p}} - 1} + \frac{v_q T^4}{2\pi^2} \int_0^\infty \frac{|\tilde{p}|^3 d\tilde{p}}{e^{\tilde{p}} + 1}. \quad (\text{A.15})$$

The final integration over \tilde{p} yields the expression

$$\epsilon = v_g \frac{\pi^2 T^4}{30} + v_q \frac{7\pi^2 T^4}{240}. \quad (\text{A.16})$$

If the degeneracy factors are again given by

$$v_g = 8_{colour} \times 2_{spin} = 16 \quad (\text{A.17})$$

$$v_q = 2_{q\bar{q}} \times 2_{spin} \times 3_{flavour} \times 3_{colour} = 36 \quad (\text{A.18})$$

the energy density becomes

$$\epsilon = \frac{19\pi^2 T^4}{12}. \quad (\text{A.19})$$

After rearranging this expression, the temperature at any given time in the evolution can be determined from

$$T = \left(\frac{\epsilon(\tau)}{(19/12)\pi^2} \right)^{1/4}. \quad (\text{A.20})$$

The temperature evolution computed using Maxwell-Boltzmann statistics was compared to that computed using Fermi-Dirac/Bose-Einstein for $Q_s = 1$ GeV. As the temperature obtained through Fermi-Dirac/Bose-Einstein statistics is only approximately 10% larger than that of Maxwell-Boltzmann statistics, the latter was used.

APPENDIX B

B.1 NUMBER DENSITY

From relativistic kinetic theory, the number density is given by

$$n_g(\tau) = \nu_g \int \frac{d^3\mathbf{p}}{(2\pi)^3} f_g(p^0) \quad (\text{B.1})$$

for gluons and

$$n_q(\tau) = \nu_q \int \frac{d^3\mathbf{p}}{(2\pi)^3} f_q(p^0) \quad (\text{B.2})$$

for quarks, where $\nu_{g/q}$ and $f_{g/q}$ the degeneracy factors and particle distribution functions for gluons and quarks respectively. Using Fermi-Dirac and Bose-Einstein statistics, the distribution functions are of the form

$$f_{q/g} = \frac{1}{e^{p^0/T} \pm 1} \quad (\text{B.3})$$

Inserting this into the above equation gives

$$n_g(\tau) = \nu_g \int \frac{d^3\mathbf{p}}{(2\pi)^3} \frac{1}{e^{p^0/T} - 1} \quad (\text{B.4})$$

$$n_q(\tau) = \nu_q \int \frac{d^3\mathbf{p}}{(2\pi)^3} \frac{1}{e^{p^0/T} + 1}. \quad (\text{B.5})$$

As in the energy density calculation in Appendix A, a change of variables to $\tilde{p} = p^0/T$ is performed the integration measure becomes $d^3\tilde{p} = |\tilde{p}|^2 d\tilde{p} d\Omega$

$$n_g(\tau) = \nu_g T^3 \int \frac{\tilde{p}^2 d\tilde{p} d\Omega}{(2\pi)^3} \frac{1}{e^{\tilde{p}} - 1} \quad (\text{B.6})$$

$$n_q(\tau) = \nu_q T^3 \int \frac{\tilde{p}^2 d\tilde{p} d\Omega}{(2\pi)^3} \frac{1}{e^{\tilde{p}} + 1} \quad (\text{B.7})$$

where integrating over solid angle gives

$$n_g(\tau) = \frac{\nu_g T^3}{2\pi^2} \int_0^\infty \frac{\tilde{p}^2 d\tilde{p}}{(2\pi)^3} \frac{1}{e^{\tilde{p}} - 1} \quad (\text{B.8})$$

$$n_q(\tau) = \frac{\nu_q T^3}{2\pi^2} \int_0^\infty \frac{\tilde{p}^2 d\tilde{p}}{(2\pi)^3} \frac{1}{e^{\tilde{p}} + 1}. \quad (\text{B.9})$$

The final integration over \tilde{p} yields the expressions

$$n_g(\tau) = 2\nu_g\zeta(3)T^3 \quad (\text{B.10})$$

$$n_q(\tau) = \nu_q \frac{3\zeta(3)T^3}{2} \quad (\text{B.11})$$

where $\zeta(3)$ is the Riemann zeta function. If the degeneracy factors are once again given by

$$\nu_g = 8_{colour} \times 2_{spin} = 16 \quad (\text{B.12})$$

$$\nu_q = 2_{q\bar{q}} \times 2_{spin} \times 3_{flavour} \times 3_{colour} = 36 \quad (\text{B.13})$$

the number densities become

$$n_g(\tau) = 32\zeta(3)T^3 \approx 38.4658T^3 \quad (\text{B.14})$$

$$n_q(\tau) = 54\zeta(3)T^3 \approx 64.9111T^3 \quad (\text{B.15})$$

Summing these two expressions gives the total number density of quarks and gluons in the QGP

$$n(\tau) = n_g(\tau) + n_q(\tau) \quad (\text{B.16})$$

$$= 86\zeta(3)T^3 \quad (\text{B.17})$$

$$\approx 103.377T^3. \quad (\text{B.18})$$

BIBLIOGRAPHY

- [1] P. M. Watkins. "DISCOVERY OF THE W AND Z BOSONS." In: *Contemp. Phys.* 27 (1986), pp. 291–324.
- [2] Joseph I. Kapusta and Charles Gale. *Finite-Temperature Field Theory: Principles and Applications*. 2nd ed. Cambridge Monographs on Mathematical Physics. Cambridge University Press, 2006.
- [3] Mark Alford. "Cool quarks." In: *Physics* 3 (2010), p. 44.
- [4] M.E. Peskin and D.V. Schroeder. *An Introduction to Quantum Field Theory*. Advanced book classics. Avalon Publishing, 1995. ISBN: 9780201503975.
- [5] Vardan Khachatryan et al. "Constraints on parton distribution functions and extraction of the strong coupling constant from the inclusive jet cross section in pp collisions at $\sqrt{s} = 7$ TeV." In: *Eur. Phys. J. C* 75.6 (2015), p. 288.
- [6] Rajan Gupta. "Introduction to lattice QCD: Course." In: *Probing the standard model of particle interactions. Proceedings, Summer School in Theoretical Physics, NATO Advanced Study Institute, 68th session, Les Houches, France, July 28-September 5, 1997. Pt. 1, 2.* 1997, pp. 83–219.
- [7] Z. Fodor and S. D. Katz. "The Phase diagram of quantum chromodynamics." In: (2009). arXiv: [0908.3341](https://arxiv.org/abs/0908.3341) [hep-ph].
- [8] A. K. Chaudhuri. *A short course on Relativistic Heavy Ion Collisions*. IOPP, 2014. arXiv: [1207.7028](https://arxiv.org/abs/1207.7028) [nucl-th].
- [9] Charles Gale, Sangyong Jeon, and Bjoern Schenke. "Hydrodynamic Modeling of Heavy-Ion Collisions." In: *Int. J. Mod. Phys. A* 28 (2013), p. 1340011.
- [10] F. Gelis. "Color Glass Condensate and Glasma." In: *Int. J. Mod. Phys. A* 28 (2013), p. 1330001.

- [11] Edward Shuryak. “Why does the quark gluon plasma at RHIC behave as a nearly ideal fluid?” In: *Prog. Part. Nucl. Phys.* 53 (2004), pp. 273–303.
- [12] Berndt Müller. “Investigation of Hot QCD Matter: Theoretical Aspects.” In: *Phys. Scripta* T158 (2013), p. 014004.
- [13] Björn Schenke, Prithwish Tribedy, and Raju Venugopalan. “Fluctuating Glasma Initial Conditions and Flow in Heavy Ion Collisions.” In: *Phys. Rev. Lett.* 108 (25 2012), p. 252301.
- [14] Bjoern Schenke, Sangyong Jeon, and Charles Gale. “(3+1)D hydrodynamic simulation of relativistic heavy-ion collisions.” In: *Phys. Rev.* C82 (2010), p. 014903.
- [15] Fred Cooper and Graham Frye. “Comment on the Single Particle Distribution in the Hydrodynamic and Statistical Thermodynamic Models of Multiparticle Production.” In: *Phys. Rev.* D10 (1974), p. 186.
- [16] S. A. Bass et al. “Microscopic models for ultrarelativistic heavy ion collisions.” In: *Prog. Part. Nucl. Phys.* 41 (1998), pp. 255–369.
- [17] Dinesh Kumar Srivastava, Bikash Sinha, Ioulia Kvasnikova, and Charles Gale. “Emission of single photons, hadrons, and dileptons in Pb + Pb collisions at CERN SPS and quark hadron phase transition.” In: *Nucl. Phys.* A698 (2002), pp. 432–435.
- [18] Ralf Rapp and Hendrik van Hees. “Thermal Dileptons as Fireball Thermometer and Chronometer.” In: *Phys. Lett.* B753 (2016), pp. 586–590.
- [19] Jean-Paul Blaizot, Bin Wu, and Li Yan. “Quark production, Bose–Einstein condensates and thermalization of the quark–gluon plasma.” In: *Nucl. Phys.* A930 (2014), pp. 139–162.
- [20] Joseph Kapusta, Peter Lichard, and David Seibert. “High-energy photons from quark-gluon plasma versus hot hadronic gas.” In: *Phys. Rev. D* 44 (9 1991), pp. 2774–2788.
- [21] K. Kajantie, J. Kapusta, L. McLerran, and A. Mekjian. “Dilepton emission and the QCD phase transition in ultrarelativistic nuclear collisions.” In: *Phys. Rev. D* 34 (9 1986), pp. 2746–2754.

- [22] J.H. Ferziger and H.G. Kaper. *Mathematical theory of transport processes in gases*. North-Holland Pub. Co., 1972.
- [23] S.R. Groot, W.A. Leeuwen, and C.G. van Weert. *Relativistic kinetic theory: principles and applications*. North-Holland Pub. Co., 1980. ISBN: 9780444854537.
- [24] Jürgen Berges, Klaus Reygers, Naoto Tanji, and Raju Venugopalan. “Parametric estimate of the relative photon yields from the glasma and the quark-gluon plasma in heavy-ion collisions.” In: *Phys. Rev. C* 95 (5 2017), p. 054904.
- [25] Larry McLerran. “The Color Glass Condensate, Glasma and the Quark Gluon Plasma in the Context of Recent pPb Results from LHC.” In: *Journal of Physics: Conference Series* 458.1 (2013), p. 012024.
- [26] C. Patrignani et al. “Review of Particle Physics.” In: *Chin. Phys.* C40.10 (2016), p. 100001.
- [27] Alfred H. Mueller. “Toward equilibration in the early stages after a high-energy heavy ion collision.” In: *Nucl. Phys.* B572 (2000), pp. 227–240.
- [28] Xu-Guang Huang and Jinfeng Liao. “Glasma Evolution and Bose-Einstein Condensation with Elastic and Inelastic Collisions.” In: *Phys. Rev.* D91.11 (2015), p. 116012.
- [29] Jean-Paul Blaizot, Francois Gelis, Jin-Feng Liao, Larry McLerran, and Raju Venugopalan. “Bose–Einstein Condensation and Thermalization of the Quark Gluon Plasma.” In: *Nucl. Phys.* A873 (2012), pp. 68–80.
- [30] L.P. Pitaevskii and E.M. Lifshitz. *Physical Kinetics*. Pergamon Press, 1981.
- [31] Jean-Paul Blaizot, Jinfeng Liao, and Larry McLerran. “Gluon Transport Equation in the Small Angle Approximation and the Onset of Bose-Einstein Condensation.” In: *Nucl. Phys.* A920 (2013), pp. 58–77.
- [32] Olaf Kaczmarek and Felix Zantow. “Quark antiquark energies and the screening mass in a quark-gluon plasma at low and high temperatures.” In: *Proceedings, Workshop on Extreme QCD, 2005*. 2005, pp. 108–112.
- [33] Alfred H. Mueller. “Parton saturation at small x and in large nuclei.” In: *Nucl. Phys.* B558 (1999), pp. 285–303.

- [34] Mauricio Martinez and Michael Strickland. "Pre-equilibrium dilepton production from an anisotropic quark-gluon plasma." In: *Phys. Rev. C* 78 (2008), p. 034917.
- [35] Charles Gale. "Photon Production in Hot and Dense Strongly Interacting Matter." In: *Landolt-Bornstein* 23 (2010), p. 445.
- [36] Jean-François Paquet, Chun Shen, Gabriel S. Denicol, Matthew Luzum, Björn Schenke, Sangyong Jeon, and Charles Gale. "Production of photons in relativistic heavy-ion collisions." In: *Phys. Rev. C* 93.4 (2016), p. 044906.